STRESS-WAVE ANALYSIS TECHNIQUE STUDY ON THICK-WALLED TYPE A302B STEEL PRESSURE VESSELS

by

C.E. Hartbower, F.J. Climent, C. Morais, P.P. Crimmins

July 1969

Prepared under Contract NAS 9-7759, Modification 1 for the
NASA Manned Spacecraft Center
Houston, Texas

Advanced Materials Technology Section
Research & Technology Department
Aerojet-General Corporation
Sacramento, California

STRESS-WAVE ANALYSIS TECHNIQUE STUDY ON THICK-WALLED TYPE A302B STEEL PRESSURE VESSELS

by

C.E. Hartbower, F.J. Climent, C. Morais, P.P. Crimmins

July 1969

Prepared under Contract NAS 9-7759, Modification 1 for the

NASA Manned Spacecraft Center

Houston, Texas

Advanced Materials Technology Section
Research & Technology Department
Aerojet-General Corporation
Sacramento, California

FOREWORD

This report was prepared by Aerojet-General Corporation, Sacramento, California under NASA Contract NAS 9-7759, Modification No. 1, during the period of July 1968 to July 1969. The work was administered under the Technical Direction of Mr. W. E. Clautice, NASA-Kennedy Space Flight Center, Florida.

The study program at the Aerojet-General Corporation was performed under the technical direction of C. E. Hartbower. Aerojet personnel who also participated in the program include W. G. Reuter, A. T. Green, C. Morais, F. J. Climent, and P. P. Crimmins of the Materials Integrity Section. All of these personnel participated in the preparation of this report.

ABSTRACT

The results of investigations to determine relationships between stress-wave-emission characteristics and subcritical crack growth in Type A302, Grade B alloy steel are presented. Stress-wave-emission characteristics which can be used as precursors for instability (failure) for unhydrogenated and hydrogenated material tested in air and 3% NaCl-water environments are discussed. The fracture behavior of unhydrogenated and hydrogenated A302B steel in these environments is also described. The results of background noise measurements at the Pad A and VAB Bottle Fields at the Kennedy Space Flight Center are presented and the feasibility of monitoring subcritical crack growth in Type A302B steel determined by correlating these results with the laboratory stress wave emission-fracture test data. Stress-wave-emission attenuation data are also presented and employed to determine sensor patterns for the pressure vessels at Pad A and the VAB Bottle Field.

TABLE OF CONTENTS

LIST OF TABLES

LIST OF FIGURES

LIST OF FIGURES (cont.)

LIST OF FIGURES (cont.)

I. INTRODUCTION

The reliability and continuous satisfactory performance of steel pressure vessels in the propellant systems of the J. F. Kennedy Space Center Launch Complex are essential to ensure personnel safety and mission reliability. To ensure continued fail-safe operation of these components, a nondestructive test technique is required which can be employed to continuously or periodically monitor the vessels and which is sensitive enough to determine if a marginal flaw possibly present in these vessels propagates during service. The Stress Wave Analysis Technique (SWAT) offers promise as a nondestructive test technique for this purpose.

Previous experience has shown that it is possible to monitor subcritical crack growth by utilizing transducers to detect stress-wave emissions which accompany the energy release occurring when a flaw propagates. This principle, coupled with seismic triangulation techniques has led to the development of the Aerojet Stress Wave Analysis Technique (SWAT), which has been employed in the monitoring of pressure vessels during hydrotest including the Polaris (Ref 1)*, LEM (Ref 2), and 260-in.-dia chambers (Ref 3). The technique has also been successfully employed as a unique laboratory test method to monitor crack growth in structural metals (Ref 4, 5, and 6) and to study the mechanism by which it occurs.

Through these studies, relationships between the onset of catastrophic failure in various structural materials and stress-wave-emission characteristics, including rate of emission and amplitude, have also been established for a number of materials. However, these previous programs have shown that it is necessary to characterize the stress-wave emissions associated with fracture for the material conditions and environments (media, loading rate, temperature, etc.) particular to each application. This is necessary because of the pronounced effect such variables exert on metal fracture, the mechanism by

*References appear at end of text.

I, Introduction (cont.)

which it occurs, and the instrumentation requirements necessary to detect such flaw growth under actual service conditions. Consequently, this program was undertaken with the following objectives:

A. Develop relationships between subcritical crack growth and stress-wave-emission characteristics in Type A302, Grade B alloy steel.

B. Characterize background noise existing in typical bottle fields at the Kennedy Space Center.

C. Determine the feasibility of monitoring subcritical crack growth in pressure vessels in bottle fields at Kennedy Space Center by correlating the results of the background noise characterization and signal attenuation tests with those obtained through laboratory tests relating stress-wave characteristics and subcritical crack growth.

II. SUMMARY

Tests were performed using unhydrogenated and hydrogenated Type A302B steel specimens exposed to air and a 3% NaCl-water environment. Both rising load to failure (air environment only) and sustained load tests were performed using the Stress Wave Analysis Technique (SWAT) and a crack-opening-displacement (COD) gage to monitor subcritical crack growth. The results of these tests showed that detectable stress-wave emissions, although of small (<0.01 g) amplitude, were observed to be associated with crack growth in this material. Under all test conditions, the stress-wave emissions were observed during rising load and when failure (instability) was imminent. Both the amplitude and rate of occurrence of stress-wave emission increased as failure was approached and could be employed as precursors of the onset of instability.

II, Summary (cont.)

During hold, varying stress-wave-emission characteristics, depending on the test conditions, were observed. When tested in an air environment in the unhydrogenated condition, neither SWE nor crack growth was observed. When hydrogenated material was tested in an air environment, a creep phenomenon, evidenced by increasing SWE count and apparent crack size, was observed. With time at hold and at applied stress intensities less than critical, the creep phenomenon eventually stopped, as did the occurrence of stress-wave emissions. Unhydrogenated material tested in 3% NaCl-water produced continuous stress-wave emission punctuated by abrupt increases in SWE count, indicating continuous crack extension with larger crack jumps corresponding to abrupt increases in SWE count. However, failure was not observed during hold when testing unhydrogenated material in salt water, or hydrogenated material in air, indicating the crack-growth rate was very low. Continuous incremental crack extension characterized by continuous SWE, interspersed by abrupt increases in SWE count indicating occasional crack jumps, was also observed in testing hydrogenated material in a 3%-NaCl-water environment. However, the crack-growth rate for the latter test condition was much faster in comparison to other test environments indicating a synergistic effect due to the combination of sea water and hydrogen in interstitial solid solution.

Background noise measurements conducted at the Pad A and VAB bottle fields at the Kennedy Space Flight Center indicated that the quiescent background noise level was much lower than the amplitude of burst-type SWE associated with crack growth in A302B steel. Thus it is possible to detect SWE associated with fracture under these conditions. Difficulty is expected in detecting such flaw growth during tank blowdown and repressurization periods. However, the blowdown and repressurization periods are of short duration and the materials behavior observed during this program indicate considerable prefailure crack growth would be expected prior to failure. Consequently, even under these conditions, significant flaw growth and/or creep could still

be detected by SWAT prior to failure, which would permit triangulation to the source and tank depressurization prior to failure. Signal attenuation evaluations performed both at the Kennedy Space Flight Center and Aerojet were used to establish sensor spacing and locations for typical vessels at both Pad A and the VAB Bottle Field.

III. LABORATORY SPECIMEN DESIGN AND TEST PROCEDURES

A. MATERIAL AND SPECIMEN CONFIGURATION

The Type A302B nickel modified steel plate (3.5-in. thick) tested in this program was supplied by the Kennedy Space Center. The material characterization data shown in Table I was also supplied by NASA. The bend specimen design shown in Figure 1 was employed for the initial stress-wave-emission/crack-growth tests performed at Aerojet; the test specimens were obtained from the surface and center locations in plate material supplied by NASA. Subsequently, Wedge Opening Loading (WOL) tests were also employed. The WOL specimen was described by Novak and Rolfe (Ref 7) and is essentially a modified compact tension specimen which can be used for K_{Iscc} environmental testing. The specimen is self-stressed with a bolt and, therefore, the loading is constant displacement, so that the initial K_I value decreases to K_{Iscc} as the crack propagates. Because the specimen is self-stressed, it can be completely divorced of all extraneous noise by encasing the loaded test specimen in a sound-proof chamber. Due to the limited amount of material available (ends of the SEN-bend specimens), the X-type WOL configuration (1 x 1 x 1.44 in.) was used as originally designed by Manjoine and shown in Figure 2.

Prior to testing, the bend specimens were precracked using an electrodynamic vibration system. During cracking, the bend specimen was gripped using a vise attachment near the specimen notch, while the other end was weighted thereby producing the maximum bending moment at the specimen notch.

TABLE I

MATERIALS CHARACTERIZATION DATA
SUPPLIED BY NASA, KENNEDY SPACE CENTER

Size of Plate:	3-7/16 x 14 x 18 in.
Specification:	A302B Nickel Modified
Heat Treatment:	1650°F/3-1/2 hr Water Quench 1125°F/5 hr draw Air Cool 1100°F/3-1/2 hr Temper Air Cool
Mechanical Properties:	F_{tu} 116.2 ksi, 115.75 ksi F_{ty} 97.5 ksi, 97.3 ksi Elong. 22.0%, 20.0% R.A. 61.0%, 57.4%

CVN (ft-lb)

+50°F	-40°F
34	21
29	21
28	18

Chemistry: C-0.23, Mn-1.16, P-0.012, S-0.019, Si-0.27, Mo-0.52, Ni-0.63, B-0.0023

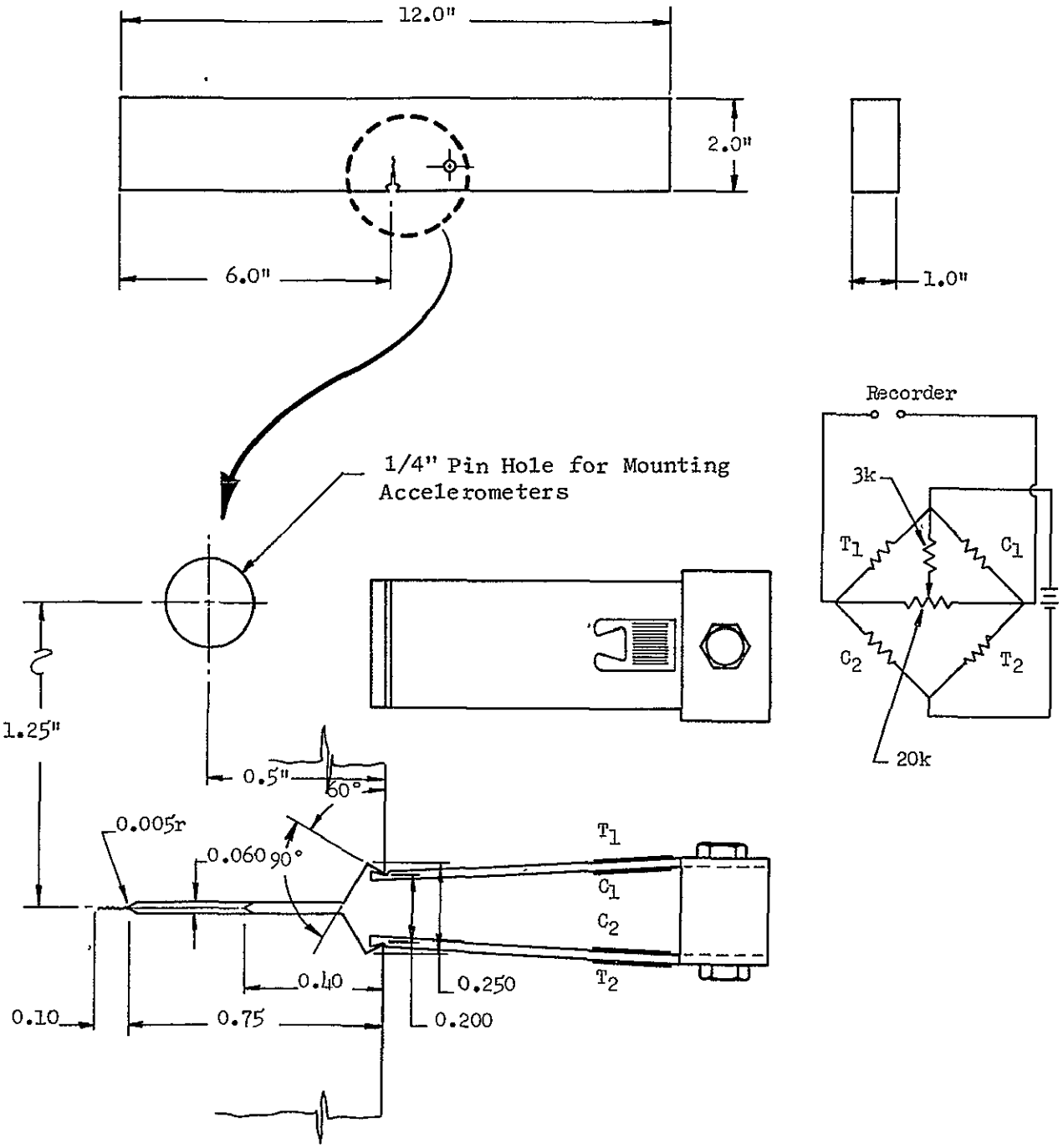

Figure 1. Notch-Bend Specimen Geometry and Crack-Opening Displacement Gage

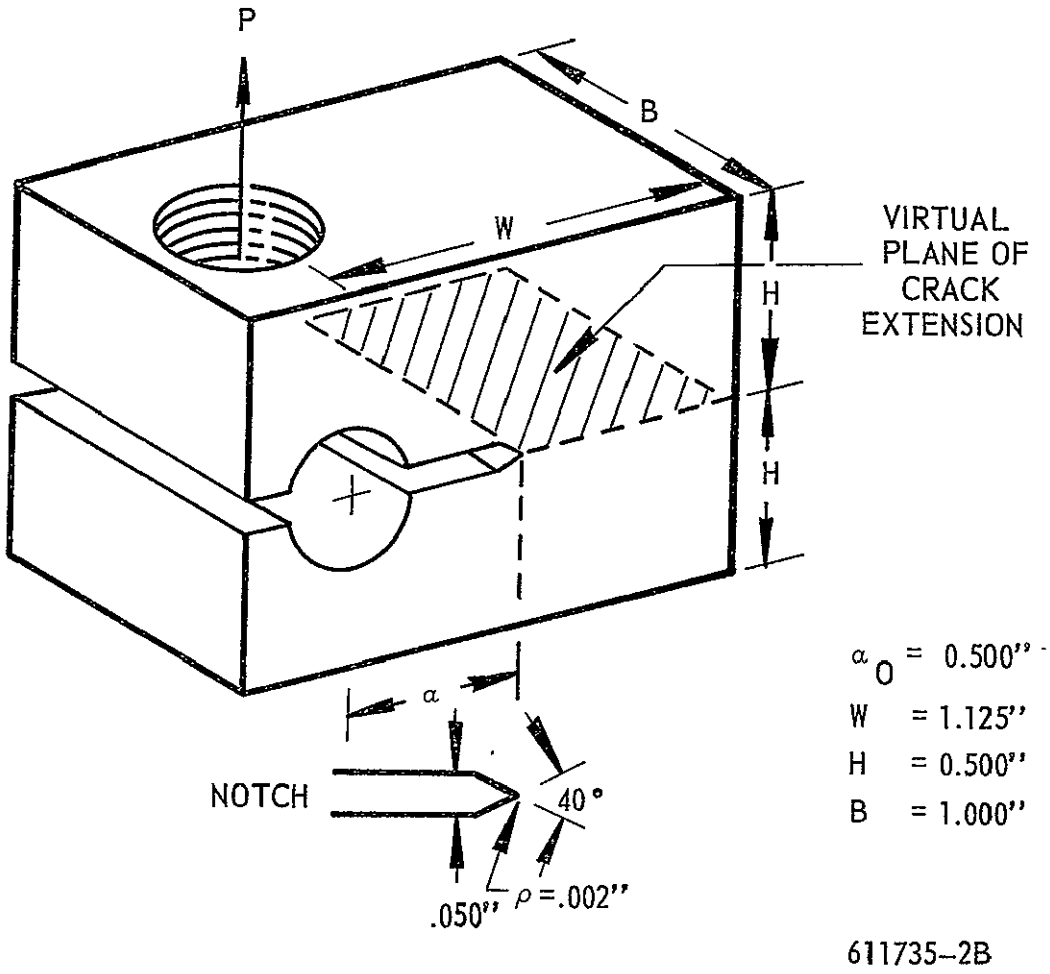

Figure 2. Configuration of WOL Specimen

III, A, Material and Specimen Configuration (cont.)

The specimen was then vibrated at resonant frequency (approximately 225 cps) until a crack approximately 0.10 in. deep appeared below the vertex of the elox-machined notch. The time required to produce the desired crack depth was approximately 10 min or 135,000 cycles. The WOL specimens were precracked (0.10-in. depth) following hydrogenation (as described in the following paragraphs) in tension-tension fatigue.

B. CRACK-OPENING DISPLACEMENT, STRESS INTENSITY, AND SPECIMEN LOADING PROCEDURE

The bend specimens were tested using the three-point bend fixture shown in Figure 3, and a hydraulic tensile machine. During loading, a crosshead speed of approximately 0.1 in./min was employed; load control during hold periods was maintained manually by the tensile machine operator. The exact specimen loading profiles varied between specimens and is discussed under the results obtained for each specimen.

During testing of the bend specimens, crack-opening displacement was measured between knife edges machined at the end of the specimen notch (Figure 1). The measuring device consisted of a full bridge of electric-resistance strain gages mounted on a double-cantilever beam. The amount of flexure in the cantilever arms was controlled by the thickness of the spacer between the arms at the base of the cantilever. The design of the gage is such that it is linear within 0.001 in. over the range of 0.200 to 0.250 in.

During the initial tests of this program, the output of the crack-opening-displacement gage was routinely recorded on a Sanborn strip chart. While this procedure is adequate for fracture toughness testing (straight rising load to failure), because of drift and normal fluctuations in output within the specification of the equipment manufacturer, this procedure is not sufficiently sensitive to detect the very small increments of crack extension

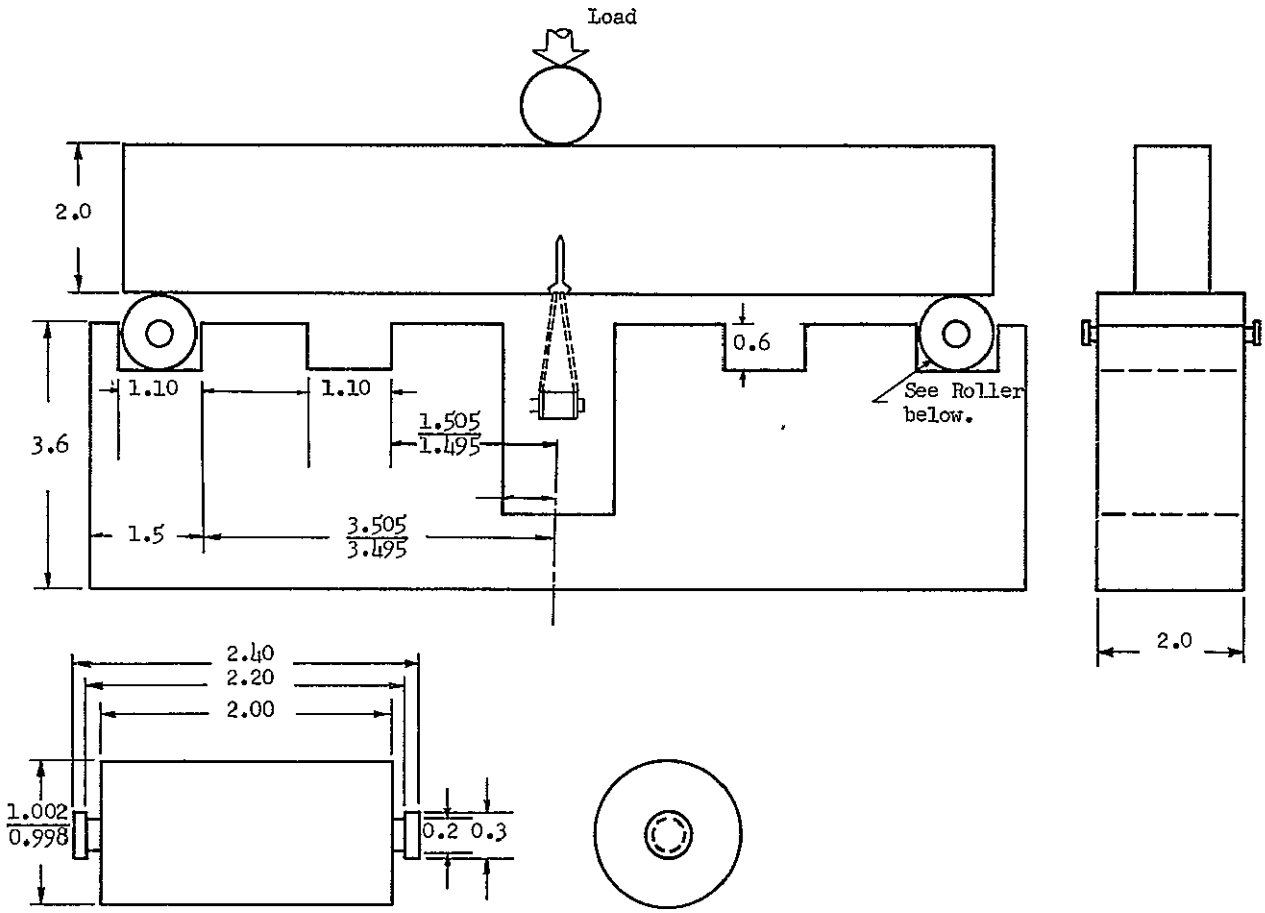

Figure 3. Three-Point Bend Test Fixture Design

which can occur during slow-crack-growth studies. This is particularly true in testing A302B steel, where extension probably occurs through a micro-void coalescence mechanism and in very small increments.

In view of this problem, a test system has been developed by Aerojet which is capable of detecting very small increments of crack extension. This system uses the crack-opening-displacement gage recommended by ASTM and described above; however, instead of a Sanborn recorder, the signal from the gage goes to a bridge balancing unit, to a DC amplifier, and then to a DC millivolt recorder. This system was operated at a gain of 1200 with less than 1% peak-to-peak instability. The system also has a zero suppression capability which allows the gain of 1200 to be fully utilized even though the crack opening may increase as much as 0.05 in. The main advantage of this system is the extremely high sensitivity capability which was required in order to detect incremental crack growth in the A302B nickel modified steel tested during this program.

The crack-opening displacements from the millivolt recorder were used to determine crack length from the notch-bend calibration curve shown in Figure 4. Stress intensity was calculated using the secant offset method recommended by the ASTM Committee for Three-Point Bend Testing. The following relationships were employed for this purpose:

$$K_Q = \frac{P_Q L}{BD^{3/2}} f(a/D) \qquad \text{(Eq 1)}$$

where L is one-half the span length, D is the specimen depth, B is the specimen thickness, a is the crack depth and P is the load at which a secant with a slope 5% less than the tangent slope interacts the load-displacement curve.

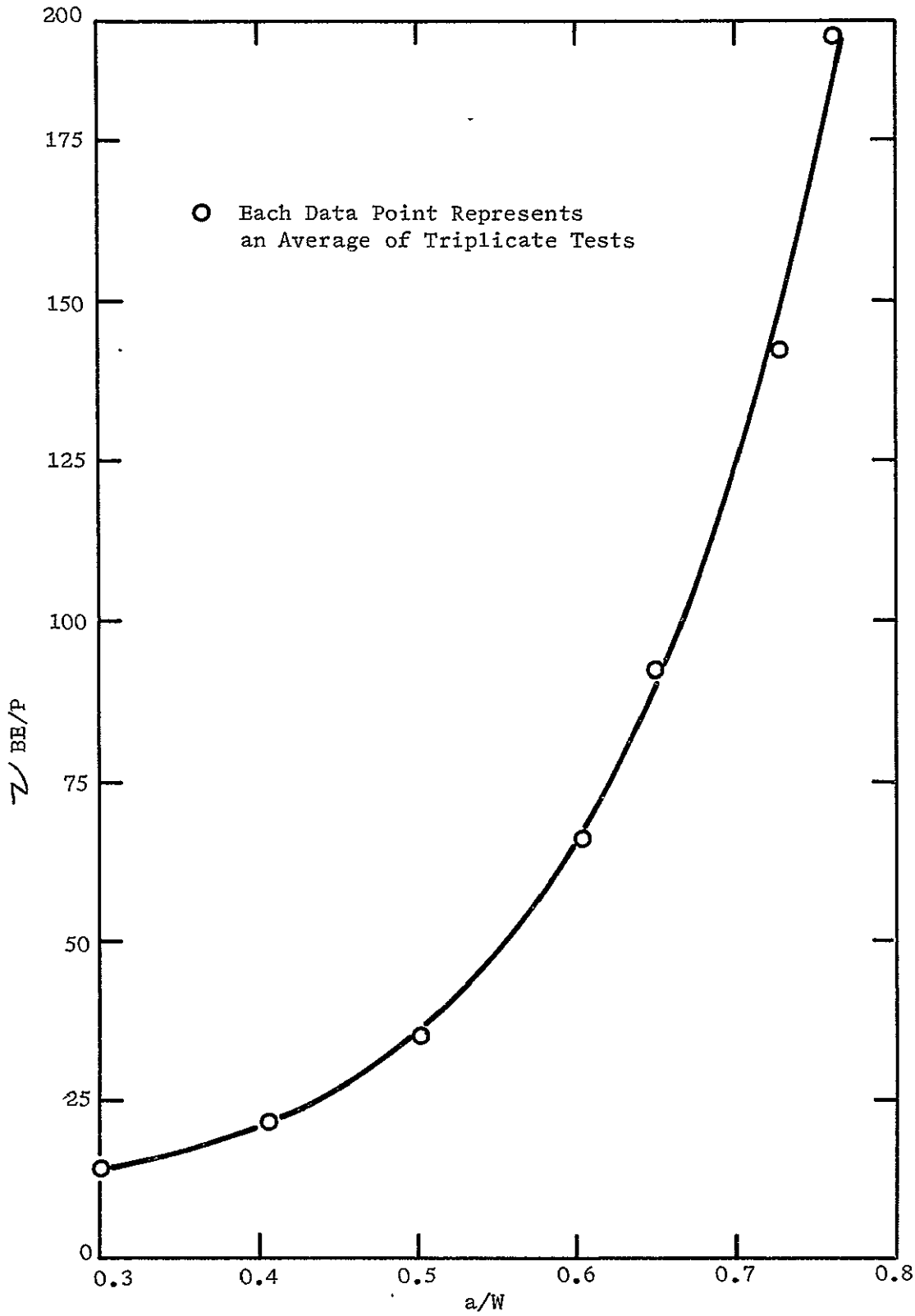

Figure 4. Calibration Curve for Three-Point Bend Specimen

III, B, Crack-Opening Displacement, Stress Intensity, and Specimen Loading Procedure (cont.)

The parameter for crack length to depth is a numerically determined polynomial given by:

$$f(a/D) = 5.8\left(\frac{a}{D}\right)^{1/2} - 9.2\left(\frac{a}{D}\right)^{3/2} + 43.6\left(\frac{a}{D}\right)^{5/2} - 75.3\left(\frac{a}{D}\right)^{7/2} + 77.4\left(\frac{a}{D}\right)^{9/2} \qquad \text{(Eq 2)}$$

The stress intensity, K_Q, is a valid K_{Ic} measurement if $2.5(K_Q/\sigma_{ys})^2$ is less than both the specimen thickness and the crack depth.

Calculation of the applied stress-intensity factor for the WOL specimen was accomplished using the following expression:

$$K_I = \frac{PC}{B\sqrt{a}} \qquad \text{(Eq 3)}$$

where P is the applied load, a is the crack depth, B is the specimen width, and C is obtained graphically from Figure 5.

Prior to precracking, the WOL specimens were hydrogenated, cadmium plated, and baked (same procedure as for the bend specimens). The specimens were then precracked (0.1 in. deep) in tension-tension fatigue. Each specimen was then calibrated by use of a crack-opening-displacement gage; this was accomplished by tensile loading the specimens and recording COD versus load with an X-Y plotter. The calibration curves for Specimen WOL-1 are shown in Figure 6. The specimens were then "self-stressed" by applying torque to the bolt (bearing against a hardened steel pin), until the COD gage indicated the desired load. The load for a given stress intensity was calculated as follows:

given $a_o' = 0.66$ in. (measured in specimen surfaces)

$W = 1.125$ in.

$a/W = 0.586$

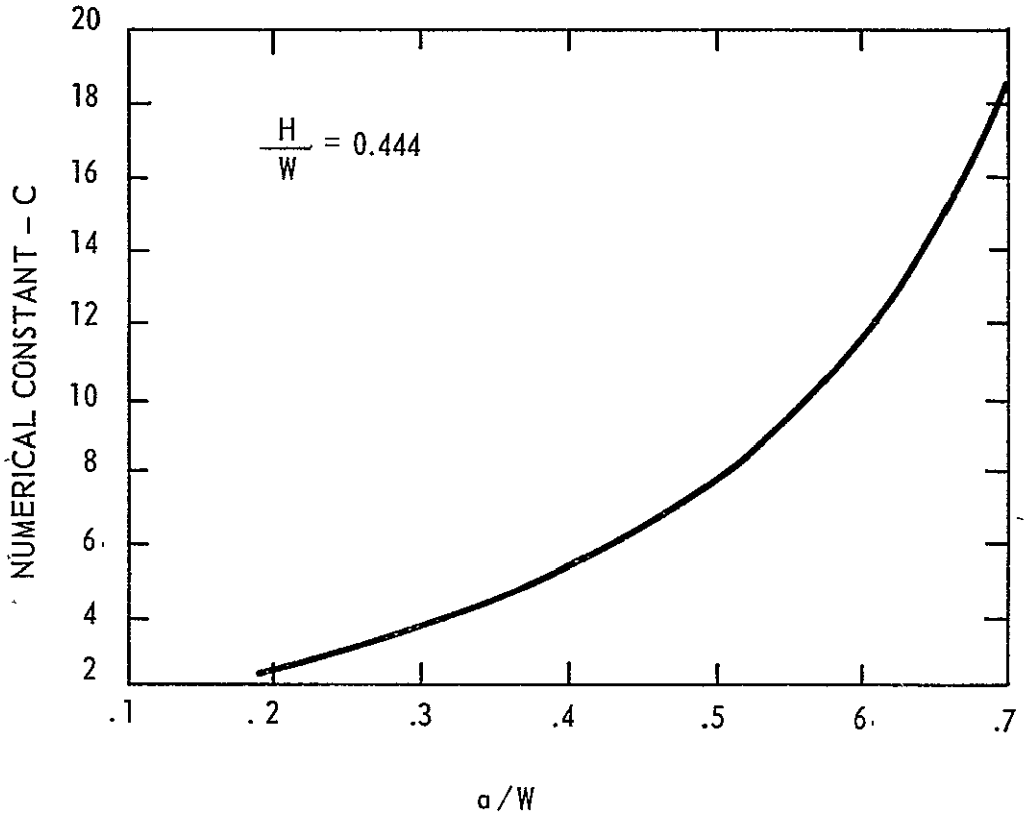

Figure 5. Numerical Constant C for WOL Specimen

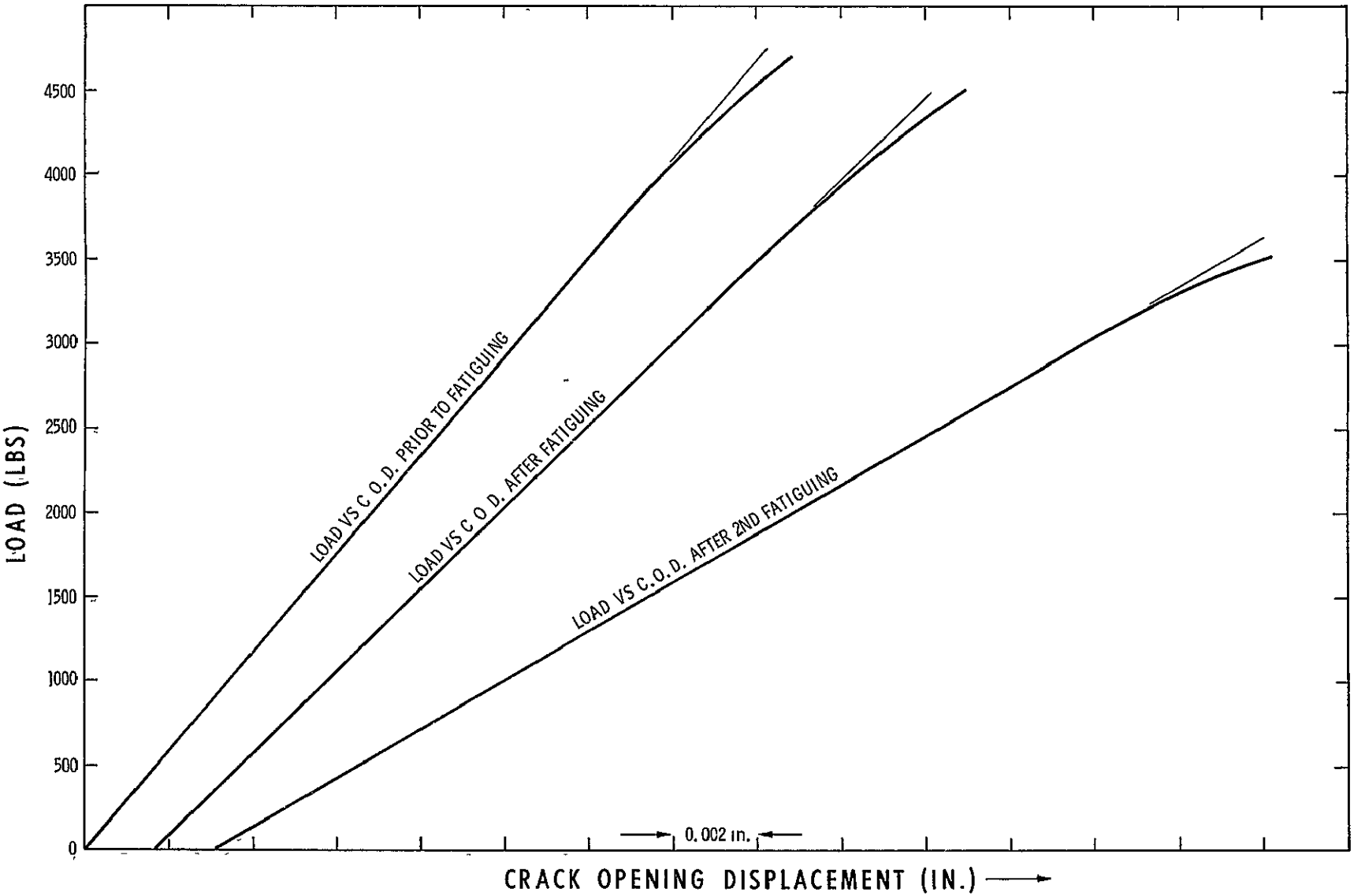

Figure 6. Crack-Opening-Displacement vs Load - WOL Specimen

III, B, Crack-Opening Displacement, Stress Intensity, and Specimen Loading Procedure (cont.)

$$C = 10.8 \text{ (graphically)}$$

$$K_I = PC/B\sqrt{a}$$

$$P = \frac{K_I B\sqrt{a}}{C}$$

for a $K_I = 50$ ksi-in.$^{1/2}$

$P = 3650$ lb

Each WOL specimen was tested with an applied load corresponding to $K_I = 50$ ksi-in.$^{1/2}$.

C. HYDROGENATION PROCEDURE

Selected bend and WOL specimens were tested after prior hydrogenation to determine the effect of this variable on the stress-wave-emission/slow-crack-growth relationships. The hydrogenation procedure employed for this purpose was developed by Battelle Memorial Institute and has been successfully employed during other programs at Aerojet. The hydrogen was introduced by cathodic charging, as follows:

Solution:	4% by weight H_2SO_4 5 drops/liter of poison
Poison:	2 gm of phosphorus dissolved in 40 ml of carbon disulphide
Charging Time:	5 min
Current Density:	10 ma/in.^{2}

The evolution of hydrogen at room temperature was prevented by cadmium plating the test specimens within 5 min after hydrogenation. The cadmium-plating procedure was as follows:

III, C, Hydrogenation Procedure (cont.)

Cadmium Plating:	4 oz/gal CdO
Solution:	16 oz/gal NaCN with 1% by volume at pH 13
Current Density:	70 ma/in.^{2}
Plating Time:	30 min

Subsequent to hydrogenation and plating, the specimens were baked at 300°F for 3 hr. Baking was performed immediately prior to testing to ensure a uniform hydrogen content throughout the test specimen.

D. STRESS-WAVE INSTRUMENTATION - LABORATORY EVALUATIONS

The stress-wave-detection system used for the laboratory evaluations prior to the background noise measurements at the Kennedy Space Center is shown schematically in Figure 7, and consists of accelerometers, amplifiers, filters, tape recorders, and an electronic counter and digital printer. During testing the accelerometers were attached to the specimens using a linear force-coiled spring technique.

Two basic systems were employed for stress-wave-emission data acquisition. During laboratory tests prior to the background measurements at Kennedy Space Center, the electronic counter system was employed. This system provides very high sensitivity (signal amplifications of 10,000 to 100,000X) and also provides a real-time automatic count (both rate of emission and cumulative count) of the stress-wave emissions occurring throughout each test period. The high-pass filter in the system eliminates a major portion of the extraneous low-frequency background noises which tend to mask very small amplitude stress waves.

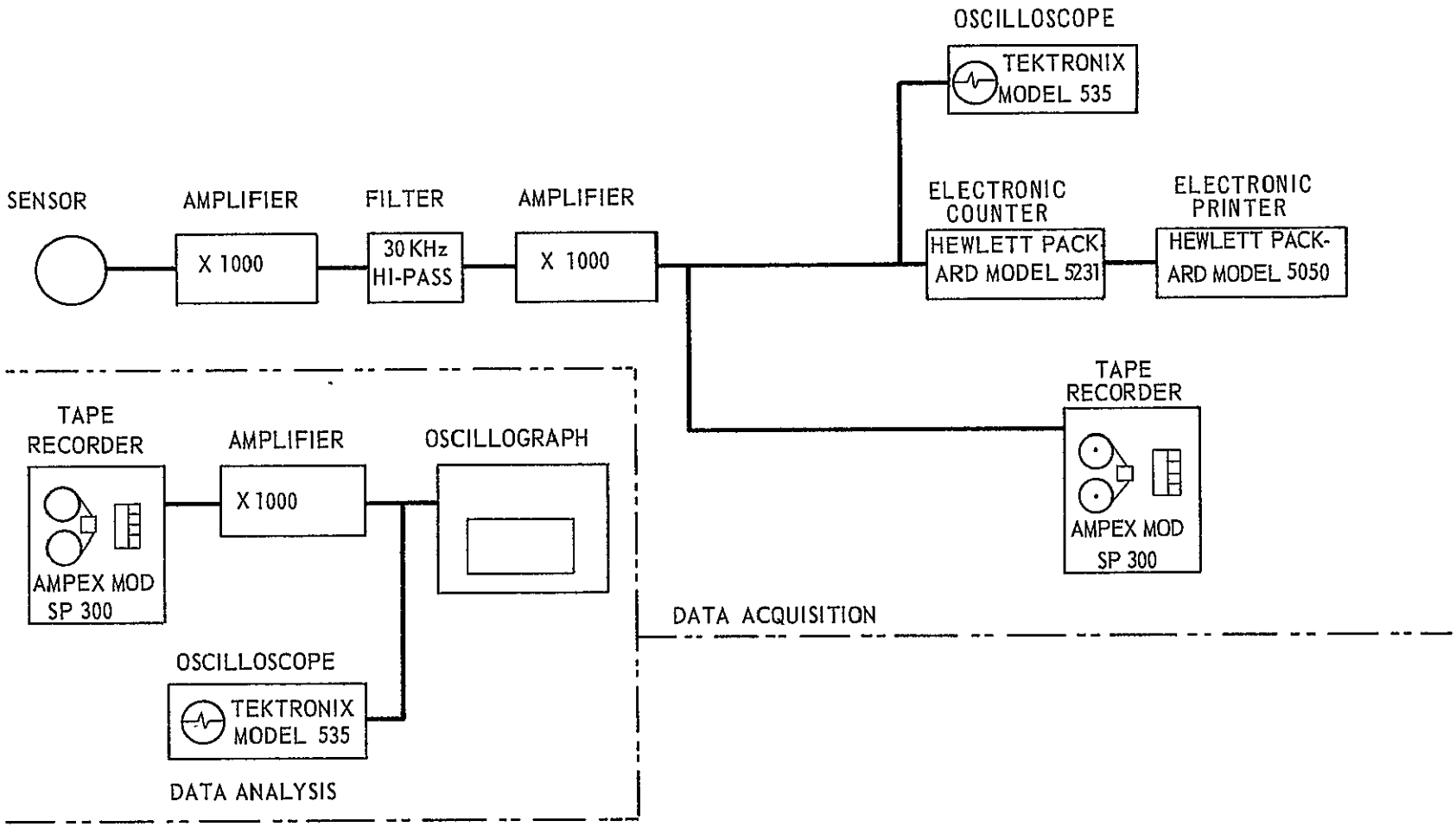

Figure 7. Schematic Representation of SWAT Data Acquisition and Data Analysis Instrumentation

III, D, Stress-Wave Instrumentation - Laboratory Evaluations (cont.)

During testing of the WOL specimens, maximum SWAT system amplification was employed. This was made possible because the specimens, immersed (COD gage up, out of the water) in the water environment, were enclosed in a sound-proof box. For these tests, the electronic counter trigger level was set just above the inherent noise (electrical) of the system. Initially, a WOL test was run to determine whether the system was in fact completely free of extraneous noise. With the COD gage connected and all recording systems in the circuit, and with the specimen under no load and in air environment, after 5-1/2 hr in the sound-proof chamber, there were only 16 signals counted. Presumably, these were electrical disturbances. The test was run during regular working hours; the WOL tests reported in the following paragraphs were run during off-hours (nights and weekends) when there should have been an absolute minimum of electrical disturbances.

A second data acquisition system was also used for a limited number of bend tests following the background noise measurements at Cape Kennedy. A schematic of this system is shown in Figure 8. The purpose of these tests was to obtain stress-wave amplitude measurements using the instrumentation employed at Cape Kennedy to ensure that the stress-wave emissions accompanying crack extension could be detected under the background conditions observed at Kennedy Space Center. The tape recordings were made by direct recording during test and were subsequently analyzed through playback and analysis as shown in Figure 7.

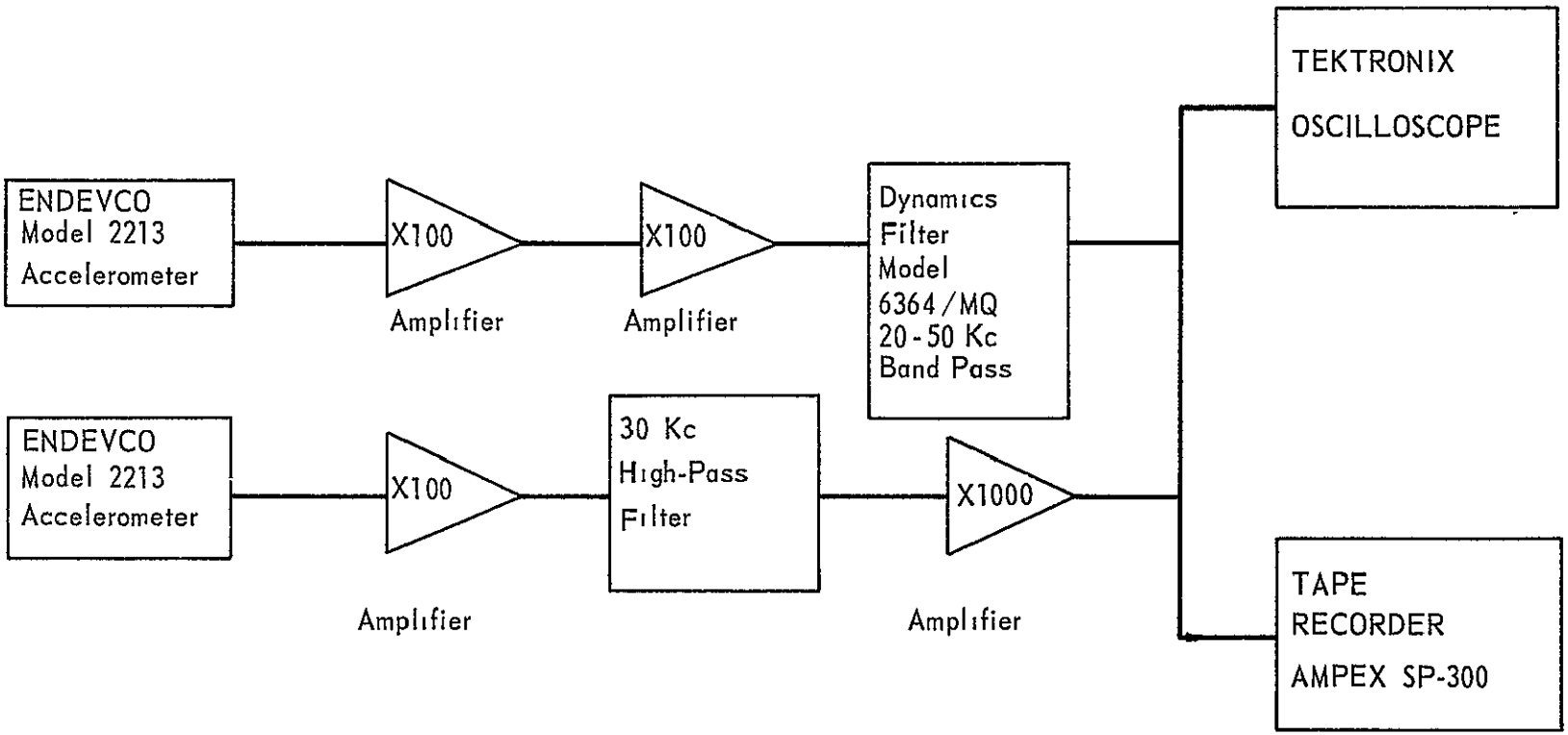

Figure 8. Schematic of Instrumentation Used at Kennedy Space Center

IV. LABORATORY TEST RESULTS AND DISCUSSION

As indicated in the following paragraphs, two environments (air and 3% NaCl-water) and two material conditions (unhydrogenated and hydrogenated) were utilized in the laboratory tests performed at Aerojet. These conditions are considered those most likely to be encountered during the service life of the pressure vessels. Also, both straight rising load to failure and sustained loading profiles were employed. The sustained load profiles were employed since failure of the pressure vessel may occur at constant load due to environmentally induced slow crack growth from a prior flaw. Since the effectiveness of a failure warning system will obviously depend on the ability to detect subcritical crack extension, whether it occurs during sustained load or on rising to failure, it is important to determine if crack extension and/or failure will occur under both conditions. Both effects can be studied through the laboratory tests performed during this program.

A. BEND TESTS IN AIR WITHOUT DELIBERATE ADDITION OF HYDROGEN

Initially, bend tests were performed in an air environment. Both the crack-opening-displacement gage and stress-wave-analysis technique were employed to monitor the occurrence of "pop-in" and subcritical crack growth. The fracture data for these tests are shown below.

No.	Specimen Thickness (B), in.	Specimen Depth (D), in.	Failure Notch Plus Fatigue Crack (a), in.	a/D	Load P, Kips	Apparent K_Q, ksi-in.$^{1/2}$
1	1.0	2.0	0.90	0.45	20.0	130
2	0.97	2.0	0.91	0.455	15.8	136
3*	1.0	2.0	1.036	0.518	16.56	133

*Intermediate hold at 123 ksi-in.$^{1/2}$

IV, A, Bend Tests in Air Without Deliberate Addition of Hydrogen (cont.)

The straight rising load to failure tests (No. 1 and 2) indicated a K_Q value of 130 to 136 ksi-in.$^{1/2}$, as did the specimen (No. 3) which failed during rising load after previous holding at a stress intensity of approximately 123 ksi-in.$^{1/2}$. As indicated previously in this report, the ASTM recommends for valid K_{Ic} measurements, a specimen thickness exceeding that corresponding to 2.5 $(K/\sigma_{ys})^2$. By this criterion, a specimen thickness of approximately 4.4 in. would be required for the A302B steel tested in this program. Consequently, the K_Q values noted above, while not "valid" K_{Ic} measurements, indicate a high level of toughness in this material.

No significant slow-crack growth or stress-wave emissions were observed during hold in the air environment. Conversely, slow-crack growth (increase in apparent crack size) and accompanying stress-wave emissions were observed during rising load to failure. The stress waves were generally very small in amplitude (<<0.01g) but increased in amplitude with increasing crack extension immediately prior to failure. Increased rate of stress-wave emission was also observed immediately prior to failure.

B. BEND TESTS IN WATER WITHOUT DELIBERATE ADDITION OF HYDROGEN

Bend specimen 4 was loaded initially to 15,000 lb (88 ksi-in.$^{1/2}$) and held at constant load for 18 hr in 3% sodium-chloride simulated sea water. The specimen showed indications of crack growth early in the hold period. However, analysis of the crack-opening-displacement gage data indicated only very small amounts of crack extension. Although the gage employed for this purpose corresponded to the design recommended by the ASTM, its use was found unsatisfactory for tests of the type performed during this program. The COD gage was then modified and the modified version used during the testing of the hydrogenated material described in subsequent sections of this report.

IV, B, Bend Tests in Water Without Deliberate Addition of Hydrogen (cont.)

When the specimens (without hydrogenation) tested in the salt-water environment were fractured, the fracture surfaces were examined for evidence of slow-crack growth during hold. Although a small band of slow-crack growth from the original fatigue precrack was observed, it was not possible to determine how much of the crack extension occurred during rising load. On the basis of the COD data, it would appear the majority of the extension occurred during rising load to 15 kips, from 15 to 17 kips, and from 17 kips to failure although the SWE data indicated that slow crack growth, however small, was occurring during the hold periods.

Figure 9 is a plot of cumulative stress-wave count over a period of approximately 1-1/2 hr during hold at 15,000 lb. Note the indications of a variable rate of subcritical crack growth. Figure 10 shows the SWAT data in detail (electronic counter reading every second) starting 23 min after reaching the 15-kip load level. Note that the cumulative stress-wave count increased more or less continuously, with brief intervals of increased slope (when plotted to the scale of Figure 10, the increased slope was approximately 45°). Figure 11 shows the SWE data obtained after adding fresh 3% NaCl-water solution to the notch. During the period of sustained load represented in Figure 11, there were a few abrupt increases in count, indicating discontinuous crack growth, together with additional intervals of increased slope (again close to 45°).

Figure 12 corresponds to the end of a short 16-kip hold (same specimen), followed by a rise to 17 kips (approximately 125 ksi-in.$^{1/2}$) and then a period of sustained load in 3% NaCl-water solution at 17 kips. Note the increased slope associated with the increase in load, followed by abrupt increases in count characteristic of discontinuous crack growth. Approximately 600 sec after starting the hold at 17 kips, an air hose produced high-frequency noise, too high to be removed by the filter. This was recorded as an abrupt increase in count, followed by a period of increased slope (again approximately 45°). It cannot be definitely stated whether the increased slope, indicating

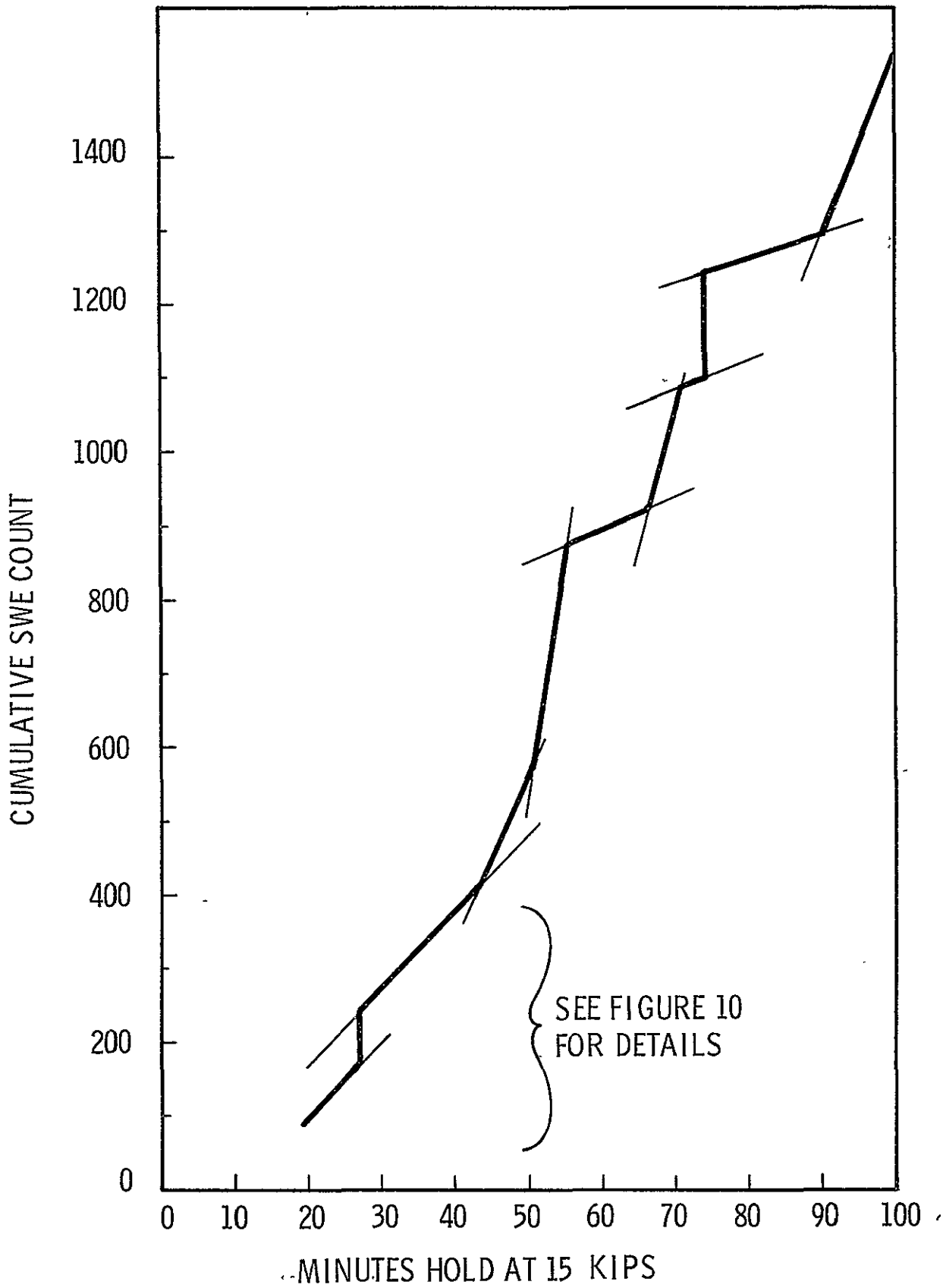

Figure 9. Cumulative Stress Wave Count vs Time, Specimen No. 4, A302B Steel, 15 Kip Hold, 3% NaCl-Water Environment

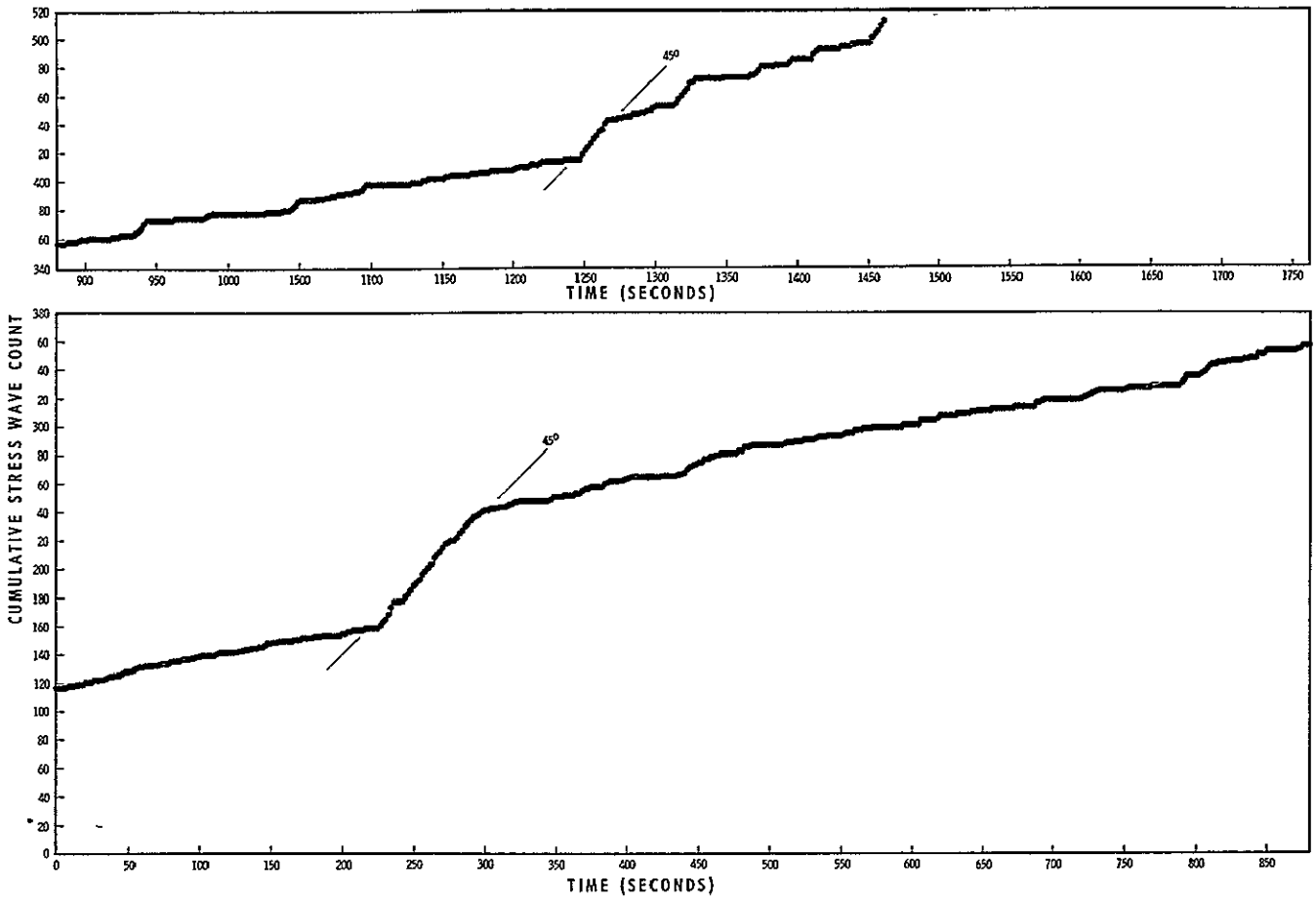

Figure 10. Cumulative Stress Wave Count vs Time, Specimen No. 4, A302B Steel, 15 Kip Hold, 3% NaCl-Water Environment

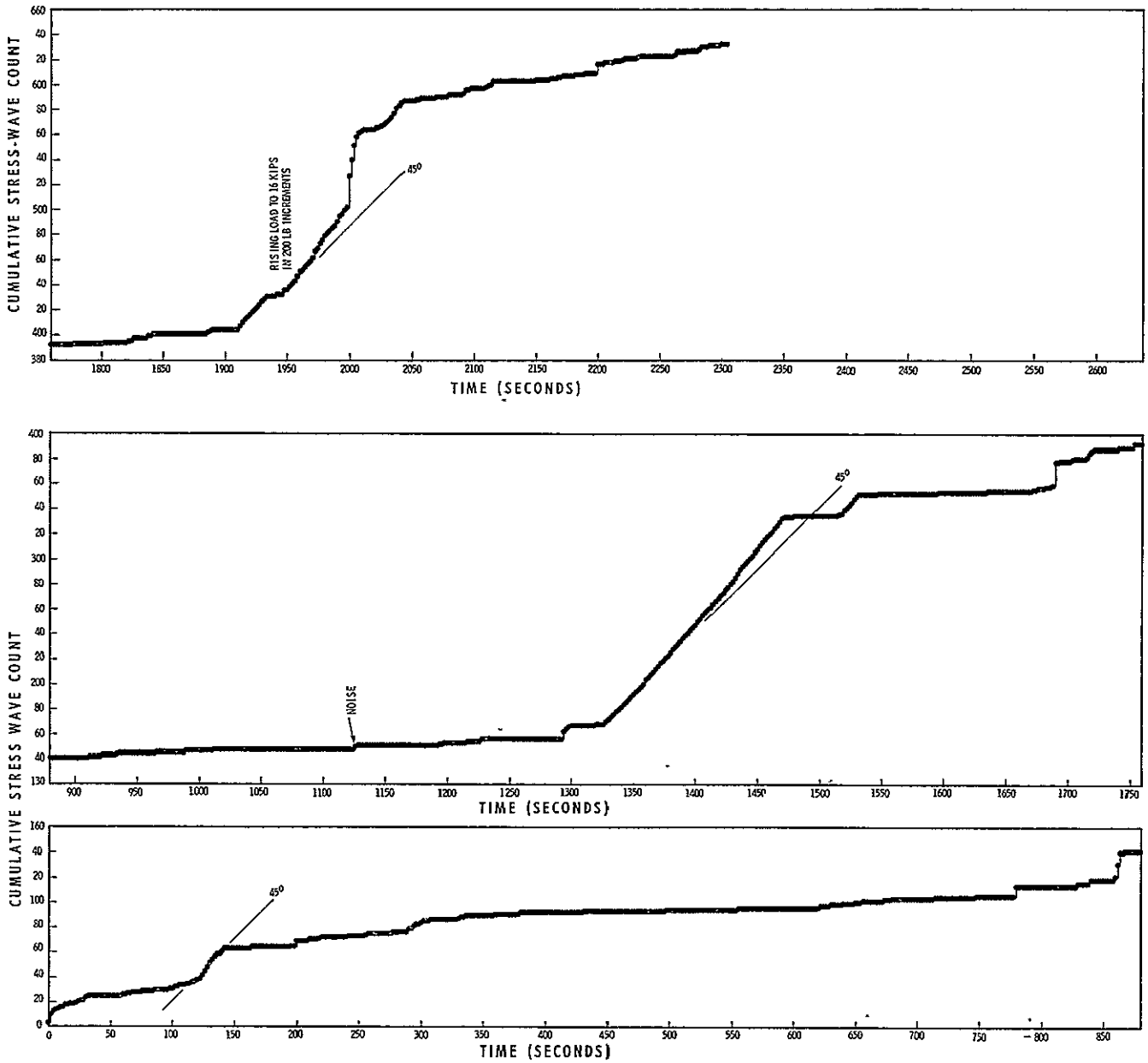

Figure 11. Cumulative Stress Wave Count vs Time, Specimen No. 4, A302B Steel, 15 Kip Hold, After Replenishing the 3% NaCl-Water Environment

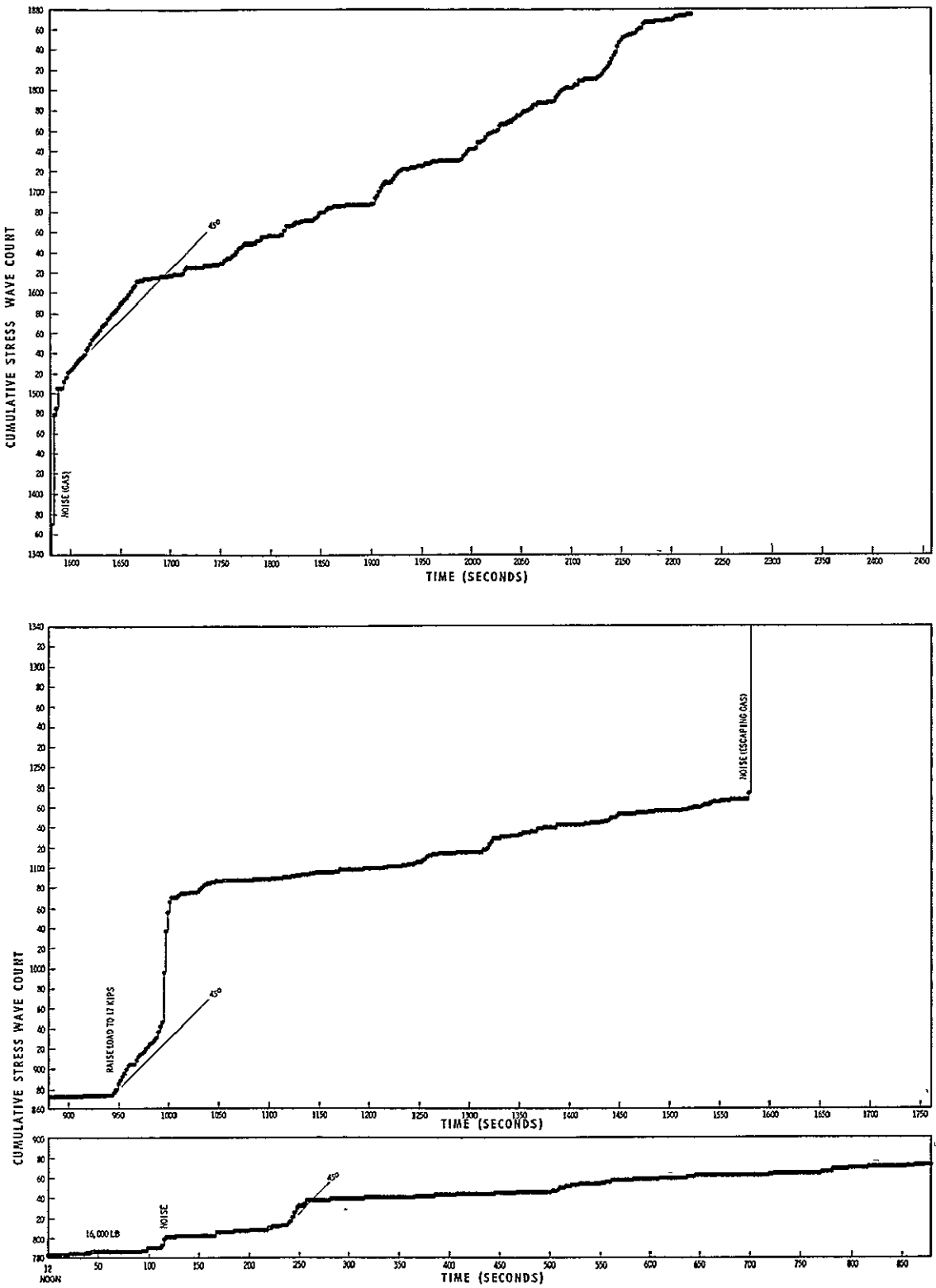

Figure 12. Cumulative Stress Wave Count vs Time, Specimen No. 4, A302B Steel, 3% NaCl-Water Environment

continuous stress-wave emission, was an artifact produced by the high-frequency noise or the increased slope was the result of crack growth stimulated by the high-frequency sound (crack growth, after periods of dormancy, can be initiated by tapping a test specimen under load). Figure 13 is a plot of the cumulative count for the 17-kip hold (corrected to zero at the start of hold and corrected for noise which occurred at 836 sec). Note the tendency for increasing slope with increasing time at load. Figure 14 presents the SWAT data in detail after 1 min at 17 kips load; Figure 15 presents the data obtained after 1-1/2 min at 17 kips load. Both Figures 14 and 15 are plotted to the same scale as Figures 10, 11, and 12. Table II presents the data plotted in Figures 13, 14, and 15, without correction for noise which occurred at 836 sec; this tabulation shows the detailed information that can be obtained by SWAT.

On the basis of the SWE data, this specimen showed evidence of very slow, continuous, crack growth of the type one might expect of electrochemical dissolution at the crack tip, interspersed with short periods of more rapid, continuous crack growth. There was little or no evidence of discontinuous crack growth with clearly defined periods of dormancy, and there were few instances of abrupt increase in count to signify crack jumps.

C. BEND TESTS IN AIR WITH DELIBERATE ADDITION OF HYDROGEN

After hydrogenation and baking 3 hr at 300°F to produce a homogeneous interstitial solid solution, specimens were tested in 70°F air. Specimen 5 (Figure 16) developed discontinuous crack growth while under sustained load starting at 9000 lb (75 ksi-in.$^{1/2}$), but the occurrences were sporadic and infrequent. At 13,000 lb (110 ksi-in.$^{1/2}$), there was only one stress wave large enough to be recorded as a cumulative count (cumulative count increased from 3086 to 3110, corresponding to 464 SWE/sec count rate). Otherwise, there was no increase in the SWE cumulative count during hold at 13,000 lb.

TABLE II

DETAILS OF SWE DATA OBTAINED FOR SPECIMEN NO. 4, A302B STEEL, DURING HOLD AT 17 KIPS IN 3% NaCl-WATER ENVIRONMENT

Time at Load (sec)	Count Rate (SWE/sec)	Cumulative Count	Interval Δt (sec)
27	57	8	-
47	134	12	20
101	4	14	54
152	3	16	51
299	10	27	147
	5 MINUTES		
329	1	29	30
357	47	37	28
444	72	49	87
460	64	56	16
494	221	60	34
511	145	62	17
	10 MINUTES		
616	115	72	105
744	128	85	128
788	2	92	44
836	2	411 (Noise)	48
838	7	411	2
843	10	431	5
845	68	431	2
846	7	431	1
855	161	447	9
880	160	468	25
	15 MINUTES		
904	11	492	24
915	209	500	11
943	5	523	28
956	22	537	13
980	4	541	24
992	13	542	12
1012	69	544	20
1088	21	558	76
1108	151	569	20
1136	111	576	28
1154	5	582	18
1172	38	583	18
1178	19	585	6
1182	9	592	4
1196	26	594	14
	20 MINUTES		
1228	80	598	32
1229	13	599	1
1238	2	605	9
1256	1	610	18
1312	91	613	56
1318	1	619	6
1321	1	621	3
1330	11	632	9
1331	20	634	1
1341	58	635	10
1392	232	652	51
1400	262	653	8
1405	134	654	5
1415	9	656	10
1443	85	657	28
1446	48	659	3
1478	131	675	32
1479	2	676	1
1495	29	685	16
	25 MINUTES		
1503	170	689	8
1505	72	691	2
1526	171	697	21
1527	1	698	1
1537	187	702	10
1546	220	705	9
1584	89	715	38
1597	119	726	13
1650	146	738	53
1666	1	749	16
1671	162	756	5
1674	86	758	3
1695	120	780	21
1708	75	782	13
1717	1	787	9
1721	84	792	4
1732	114	794	11
	30 MINUTES		
1808	228	803	76
1821	179	805	13
1825	22	808	4
1833	196	809	8
1839	120	811	6
1852	45	814	13
1866	146	816	14
1888	168	819	22
1895	14	823	7
1909	157	826	14
1933	29	832	24
1950	10	836	17
1956	46	837	6
1977	71	838	21
1988	101	839	11
2000	10	841	12

TABLE II (cont.)

Time at Load (sec)	Count Rate (SWE/sec)	Cumulative Count	Interval Δt (sec)
2002	59	843	2
2017	119	845	15
2020	148	847	3
2033	165	848	13
2039	103	850	6
2048	9	857	9
2061	129	860	13
2063	156	862	2
2069	167	864	6
2075	98	874	6
2076	3	879	1
2093	21	881	17
	35 MINUTES		
2107	1	883	14
2108	103	884	1
2118	121	885	10
2119	191	887	1
2135	154	891	16
2140	11	892	5
2146	3	894	6
2150	178	897	4
2159	51	902	9
2162	7	905	3
2180	57	909	18
2182	58	910	2
2193	17	913	11
2195	113	916	2
2207	115	919	12
2221	34	923	14
2223	87	926	2
2238	35	936	15
2258	2	943	20
2268	204	947	10
2289	10	949	21
2307	1	952	18
2319	121	955	12
2346	20	959	27
2366	69	963	20
2386	20	975	20
2387	5	976	1
2392	158	978	5
2396	8	981	4
	40 MINUTES		
2403	21	983	7
2409	241	986	6
2449	95	996	40
2457	24	998	8
2473	104	1002	16
2481	3	1003	8
2515	40	1013	34
2518	207	1017	3
2521	1	1023	3
2525	602	1029	4
2527	22	1034	2
2548	52	1052	21
2561	47	1058	13
2573	17	1062	12
2585	69	1072	12
2588	42	1073	3
2599	240	1075	11
2605	4	1077	6
2615	23	1078	10
2616	57	1079	1
2613	11	1080	15
2638	42	1081	7
2648	2	1087	10
2650	87	1088	2
2653	100	1089	3
2656	56	1090	3
2661	63	1091	5
2685	28	1094	24
2693	35	1097	8
	45 MINUTES		
2701	113	1104	8
2703	50	1105	2
2713	53	1109	10
2719	20	1110	6
2721	33	1112	2
2738	72	1115	17
2740	15	1116	2
2752	100	1117	12
2756	85	1119	4
2768	56	1121	12
2780	13	1130	12
2782	28	1135	2
2795	60	1142	13
2809	65	1144	14
2841	55	1156	32
2848	3	1157	7
2851	2	1159	3
2862	45	1163	11
2869	35	1166	7
2879	18	1169	10
2885	62	1171	6
2905	55	1175	20
2908	54	1178	3
2918	7	1182	10
2924	8	1186	6

TABLE II (cont.)

Time at Load (sec)	Count Rate (SWE/sec)	Cumulative Count	Interval Δt (sec)
2938	12	1193	14
2948	95	1201	10
2966	10	1215	18
2968	43	1216	2
2972	22	1217	4
2979	8	1221	7
2987	8	1223	8
2998	38	1226	11
	50 MINUTES		
3002	36	1228	4
3010	55	1230	8
3011	3	1234	1
3016	1	1236	5
3017	3	1237	1
3023	3	1239	6
3029	3	1240	6
3033	1	1243	4
3036	110	1245	3
3037	4	1248	1
3053	83	1259	16
3054	7	1260	1
3061	2	1265	7
3062	83	1266	1
3076	62	1275	14
3080	5	1278	4
3098	32	1294	18
3100	15	1296	2
3102	16	1297	2
3108	7	1299	6
3114	7	1301	6
3127	6	1304	13
3129	1	1305	2
3133	1	1306	4
3140	5	1309	7
3154	30	1312	14
3170	6	1320	16
3175	77	1322	5
3177	110	1323	2
3178	5	1324	1
3183	4	1326	5
3187	137	1331	4
3191	14	1332	4
3200	3	1336	9
3206	2	1340	6
3214	20	1343	8
3219	22	1345	5
	55 MINUTES		
3341	207	1410	-
3366	103	1421	25
3377	8	1424	11
3378	12	1425	1
3390	2	1429	12
3396	3	1430	6
3397	14	1432	1
3401	8	1434	4
3402	98	1438	1
3408	12	1443	6
3410	16	1448	2
3413	6	1452	3
3431	2	1454	8
3433	17	1458	2
3435	30	1460	2
3438	22	1462	3
3450	8	1475	12
3455	62	1484	5
3461	154	1490	6
3462	7	1493	1
3466	11	1501	4
3472	2	1507	6
3476	46	1509	4
3489	18	1515	13
3490	8	1517	1
3508	15	1534	18
3513	25	1541	5
3520	220	1549	7
3538	29	1566	18
3542	9	1572	4
3543	107	1575	1
3558	240	1588	15
3568	30	1601	10
3570	21	1603	2
3573	66	1607	3
3579	9	1613	6
3591	37	1619	12
	60 MINUTES		
3607	128	1622	16
3608	70	1626	1
3609	2	1629	1
3624	50	1638	15
3630	14	1642	6
3639	86	1645	9
3660	56	1662	21
3678	13	1669	18

TABLE II (cont.)

Time at Load (sec)	Count Rate (SWE/sec)	Cumulative Count	Interval Δt (sec)
3688	33	1680	10
3692	35	1682	4
3709	209	1688	17
3712	7	1689	3
3720	78	1691	8
3730	93	1694	10
3731	5	1695	1
3743	13	1703	12
3744	120	1709	1
3750	24	1715	6
3755	142	1724	5
3767	45	1738	12
3796	69	1770	29
3823	21	1808	27
3844	10	1838	21
3854	82	1851	10
3856	13	1855	2
3895	75	1915	39
	65 MINUTES		
3901	18	1920	6
3905	54	1927	4
3946	58	1963	41
3970	2	1985	24
3971	181	1988	1
3974	61	1990	3
3975	28	1992	1
3987	51	2004	12
4012	2	2022	25
4013	31	2026	1
4022	7	2036	9
4054	4	2062	32
4056	16	2066	2
4084	37	2093	28
4091	36	2099	7
4100	3	2111	9
4129	16	2142	29
4156	6	2165	27
	70 MINUTES		
4241	19	2253	85
4292	4	2299	51
4331	42	2339	39
4338	19	2348	7
4340	66	2350	2
4345	10	2359	5
4385	4	2419	40
4397	121	2432	12
	75 MINUTES		
4500	40	2534	103
4507	6	2542	7
4535	105	2574	28
4547	3	2589	12
4583	4	2616	36
4623	460	2670	40
4624	37	2703	1
4626	18	2715	2
4627	840	2729	1
4630	141	2737	3
4662	2	2758	32
4671	1	2763	9
4698	1	2774	27
4710	8	2782	12
4719	6	2784	9
4731	128	2785	12
4761	17	2810	30
4783	22	2822	22
4786	23	2824	3
	80 MINUTES		
4822	96	2831	36
4852	1	2842	30
4934	59	2890	82
4953	200	2907	19
4954	26	2910	1
4957	16	2916	3
4964	56	2923	7
4988	29	2941	24
5000	88	2951	12
5031	10	2977	31
5032	9	2978	1
5045	56	2982	13
5054	4	2984	9
5093	220	2992	39
	85 MINUTES		
5122	115	2996	29
5166	17	3019	44
5190	172	3042	24
5193	55	3045	3
5194	2	3048	1
5224	313	3081	30
5248	23	3106	24
5266	32	3123	18
5281	24	3138	15
5291	10	3150	10
5303	25	3164	12
5306	1	3169	3
5324	56	3187	18
5330	58	3193	6
5345	31	3211	15
5351	155	3217	6

TABLE II (cont.)

Time at Load (sec)	Count Rate (SWE/sec)	Cumulative Count	Interval Δt (sec)
5357	211	3223	6
5363	29	3233	6
5364	20	3237	1
	90 MINUTES		
5403	118	3276	39
5418	79	3295	15
5419	44	3298	1
5420	35	3300	1
5448	27	3324	28
5460	118	3327	12
5466	97	3329	6
5472	184	3331	6
5484	28	3333	12
5499	45	3338	15
5505	2	3341	6
5506	173	3344	1
5512	72	3346	6
5515	8	3348	3
5536	199	3352	21
5548	5	3356	12
5553	199	3359	5
5554	34	3360	1
5587	190	3364	33
5593	2	3365	6
5605	6	3367	12
5611	12	3369	6
5638	3	3373	27
5644	57	3374	6
5645	78	3376	1
5669	21	3379	24
5693	22	3384	24
5699	48	3385	6
	95 MINUTES		
5702	74	3387	3
5703	85	3389	1
5725	21	3391	22
5737	1	3394	12
5752	72	3396	15
5761	106	3398	9
5788	1	3414	27
5794	176	3422	6
5809	2	3441	15
5810	15	3445	1
5813	42	3448	3
5814	189	3451	1
5823	180	3461	9
5832	171	3472	9
5838	46	3481	6
5859	63	3505	21
5865	15	3511	6
5886	2	3533	21
5887	185	3536	1
5905	65	3559	18
5923	31	3575	18
5924	22	3576	1
5933	109	3578	9
5934	5	3579	1
5961	43	3582	27
	100 MINUTES		
6000	23	3585	39
6001	13	3586	1
6002	166	3588	1
6008	9	3590	6
6032	29	3592	24
6041	111	3596	9
6062	116	3601	21
6083	1	3603	21
6084	236	3606	1
6090	140	3607	6
6091	104	3608	1
6106	21	3609	15
6115	31	3611	9
6121	29	3614	6
6124	1	3622	3
6139	51	3630	15
6160	25	3634	21
6175	5	3636	15
6184	196	3639	9
6217	275	3645	33
6223	84	3648	6
6238	23	3649	15
6244	99	3650	6
6250	81	3652	6
6259	39	3654	9
6265	15	3656	6
6271	21	3658	6
6283	85	3660	12
	105 MINUTES		
6304	143	3662	21
6331	50	3672	27
6340	179	3674	9
6341	37	3675	1
6365	34	3677	24
6366	111	3680	1
6393	150	3682	27
6405	43	3684	12
6429	4	3687	24
6435	127	3690	6
6459	31	3691	24
6483	7	3694	24
6495	30	3696	12
6501	128	3700	6

TABLE II (cont.)

Time at Load (sec)	Count Rate (SWE/sec)	Cumulative Count	Interval Δt (sec)
6522	87	3703	21
6531	16	3704	9
6555	102	3706	24
6567	7	3709	12
6570	10	3710	3
6576	87	3711	6
6577	89	3713	1
6578	131	3714	1
6599	4	3717	21
	110 MINUTES		
6600	8	3718	1
6603	37	3720	3
6639	15	3724	36
6669	48	3728	30
6675	23	3729	6
6684	57	3731	9
6705	23	3757	21
6744	53	3807	39
6762	240	3830	18
6783	5	3854	21
6801	26	3874	18
6822	181	3901	21
6852	24	3934	30
6879	44	3962	27
6882	2	3965	3
	115 MINUTES		
6906	63	3991	24
6927	176	4001	21
6930	15	4006	3
6931	54	4011	1
6952	305	4026	21
6953	40	4033	1
6980	3	4037	27
6989	99	4039	9
7040	387	4080	51
7041	53	4095	1
7056	23	4100	15
7086	354	4108	30
7095	21	4110	9
7125	70	4117	30
7131	2	4120	6
7167	97	4129	36
7176	11	4130	9
7197	18	4133	21
	120 MINUTES		
7218	28	4136	21
7227	39	4138	9
7248	72	4146	21
7272	50	4153	24
7278	21	4158	6
7302	2	4174	24
7303	3	4174	1
7318	125	4186	15
7348	88	4205	30
7402	86	4238	54
7435	90	4258	33
7447	14	4262	12
7474	14	4277	27
7486	9	4286	12
	125 MINUTES		
7504	89	4304	18
7510	39	4308	6
7531	52	4331	21
7540	208	4344	9
7549	38	4353	9
7576	72	4376	27
7594	24	4392	18
7603	55	4403	9
7615	160	4415	12
7621	134	4420	6
7627	160	4423	6
7639	180	4430	12
7648	5	4432	9
7658	100	4437	10
7679	319	4445	21
7694	72	4449	15
7709	23	4451	15
7721	34	4453	12
	130 MINUTES		
7800	Test Terminated		

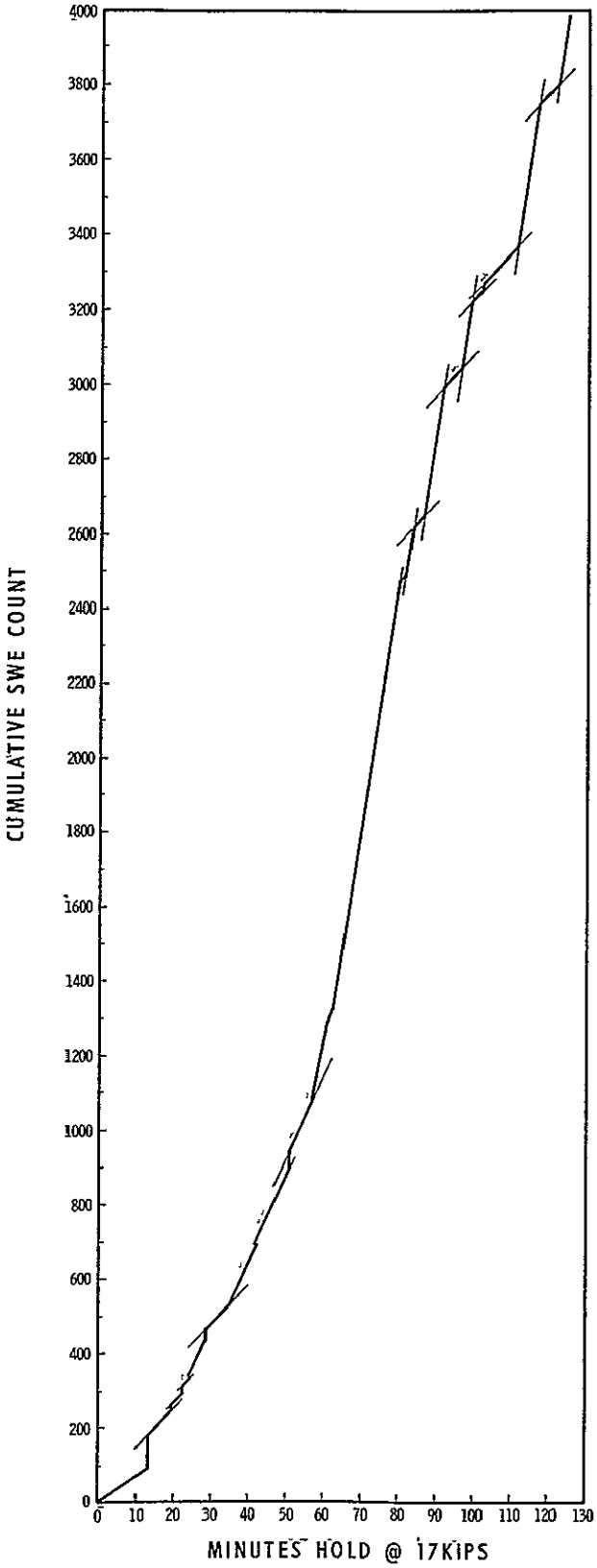

Figure 13. Cumulative Stress Wave Count vs Time, Specime A302B Steel, 3% NaCl-Water Environment

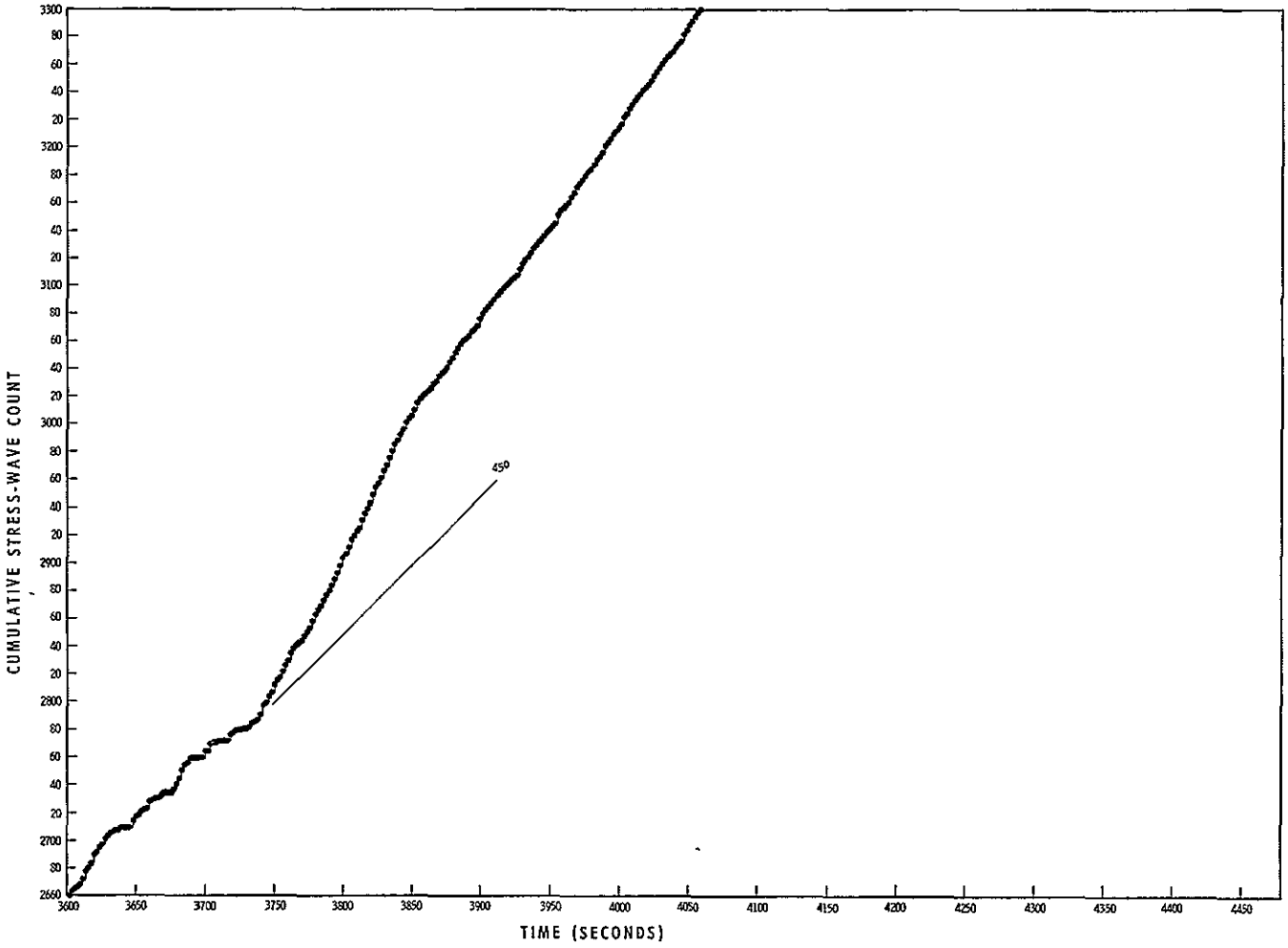

Figure 14. Cumulative Stress Wave Count vs Time, Specimen No. 4, A302B Steel, After 1 Minute at 17 Kip Hold in 3% NaCl-Water Environment

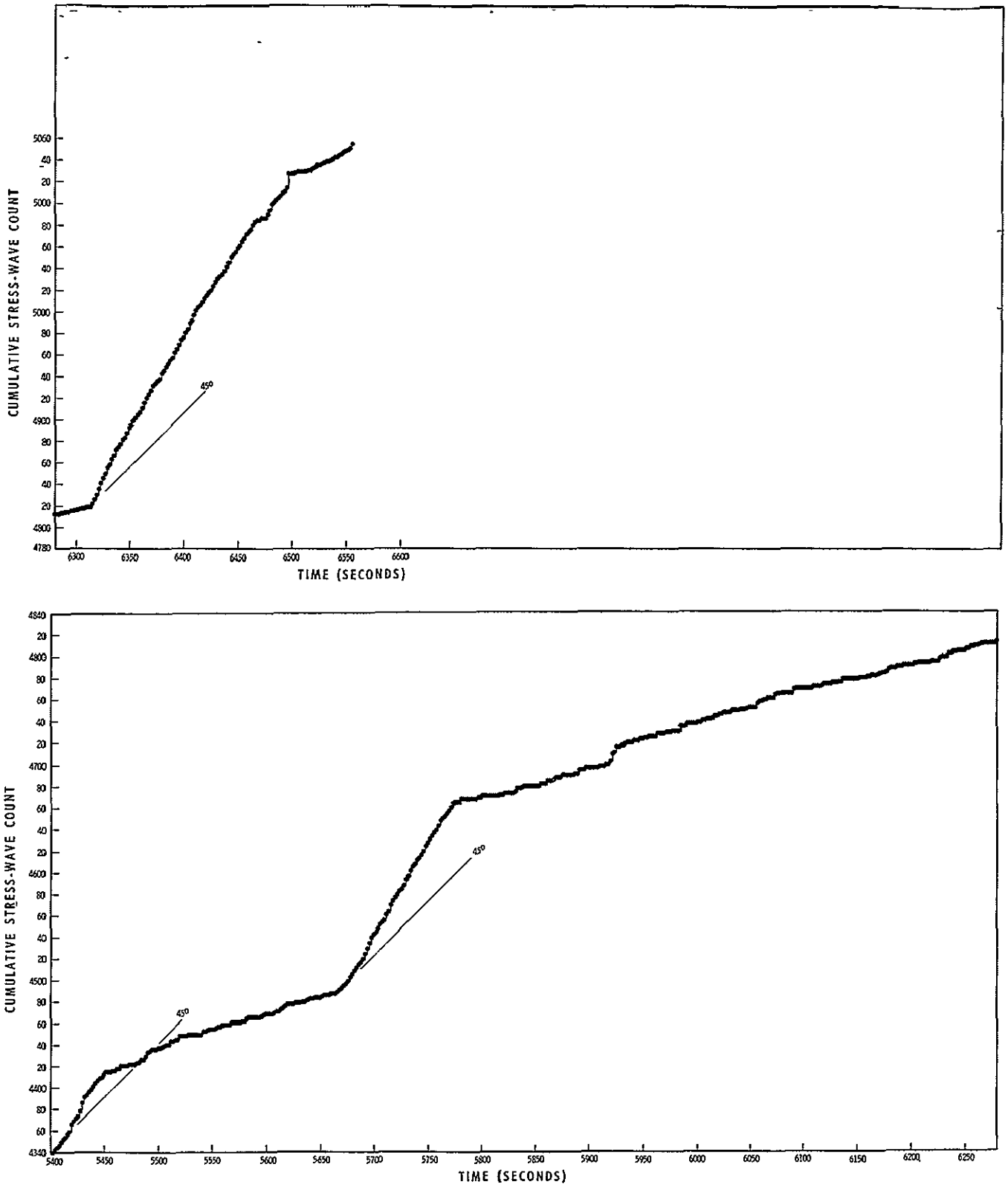

Figure 15. Cumulative Stress Wave Count vs Time, Specimen No. 4, A302B Steel, After 1-1/2 Minutes at 17 Kip Hold in 3% NaCl-Water Environment

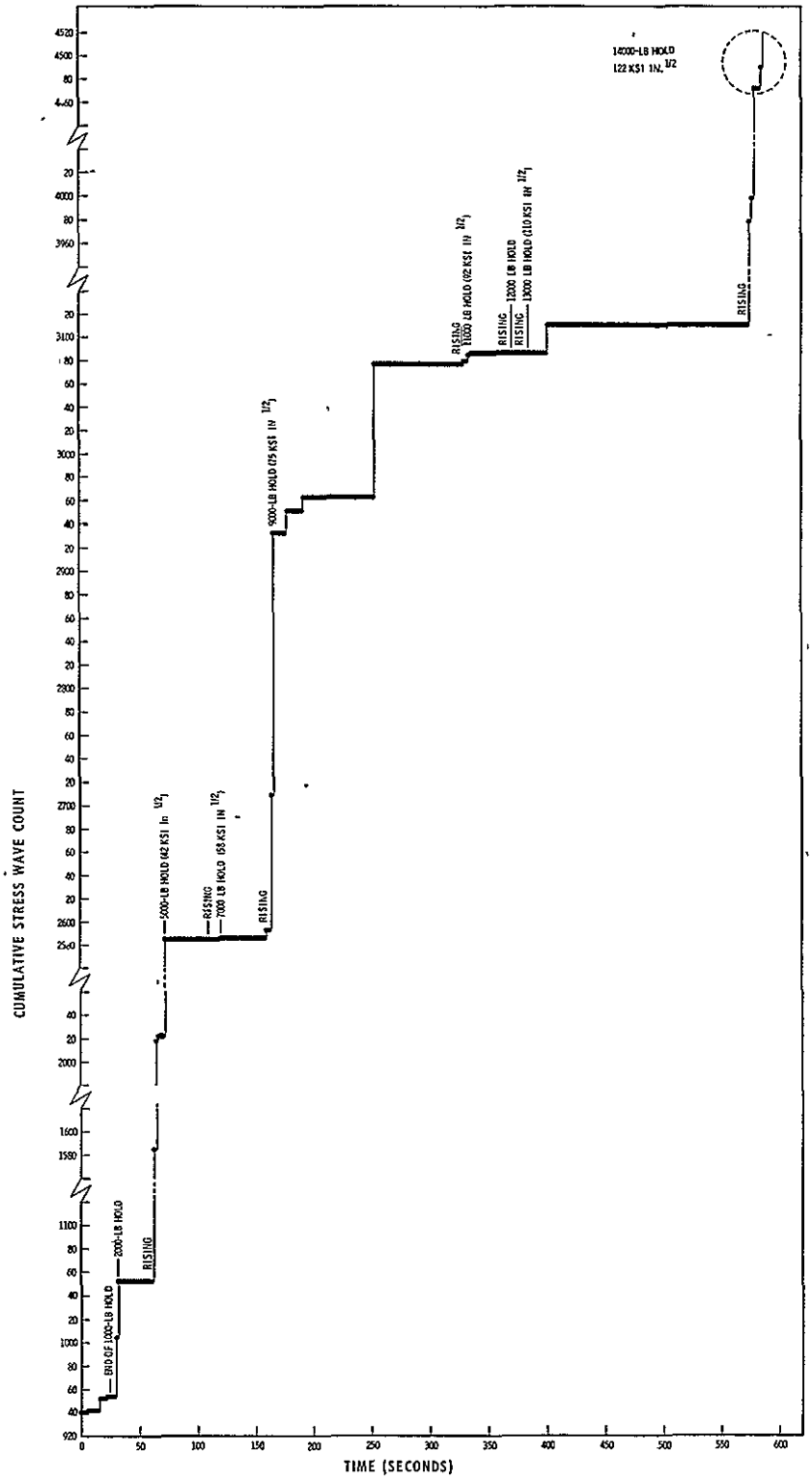

Figure 16. Cumulative Stress Wave Count vs Time, Specimen No. 5, A302B Steel, Hydrogenated and Tested in Air

IV, C, Bend Tests in Air With Deliberate Addition of Hydrogen (cont.)

On raising the load from 13,000 to 14,000 lb (122 ksi-in.$^{1/2}$), there was evidence of a "creep" phenomenon as shown in Figure 17. The crack-opening-displacement gage confirmed the occurrence of crack growth continuing after reaching the 14,000-lb hold. Stress-wave emission showed the mechanism to be discontinuous cracking rather than a deformation process. When the count rate was plotted as in Figure 18, the activity carrying into the 14,000-lb hold again was discontinuous. After approximately 300 sec at 14 kips, the SWE associated with the creep phenomenon had subsided. During the 14-kip hold, there were two crack jumps, one after 920 sec (cumulative count increased from 5618 to 5720 and the count rate associated with the jump was 181 as counted over a 10-sec interval, or 18 SWE/sec), and one after 2130 sec (cumulative count increased from 5721 to 5755 and the count rate was 139 in 10 sec).

After 5000 sec at 14 kips, the load on Specimen 5 was raised. As seen in Figure 19, the stress-wave activity was an unmistakable presage of instability which occurred after 20 sec into hold. The load reached a maximum of 14.5 kips (145 ksi-in.$^{1/2}$). Technically, the onset of instability occurred shortly after starting to increase the load; i.e., at approximately 132 ksi-in.$^{1/2}$ which agrees with the K_Q value obtained through rising load tests of unhydrogenated material in an air environment.

Because of the very long test period and multiple loadings involved in the testing of the Specimen 6, only data obtained during rising load to 19,500 and 19,800 lb, during sustained test periods at these loads, and during specimen failure are shown in Figure 20. These data indicate essentially the same SWE-crack growth relationships discussed previously for Specimen 5, except that on reaching hold, the crack tended to grow slowly for a longer period of time in comparison to the behavior noted for Specimen 5. Also, the incremental nature of crack extension was more readily observed by the stress-wave-emission data for Specimen 6.

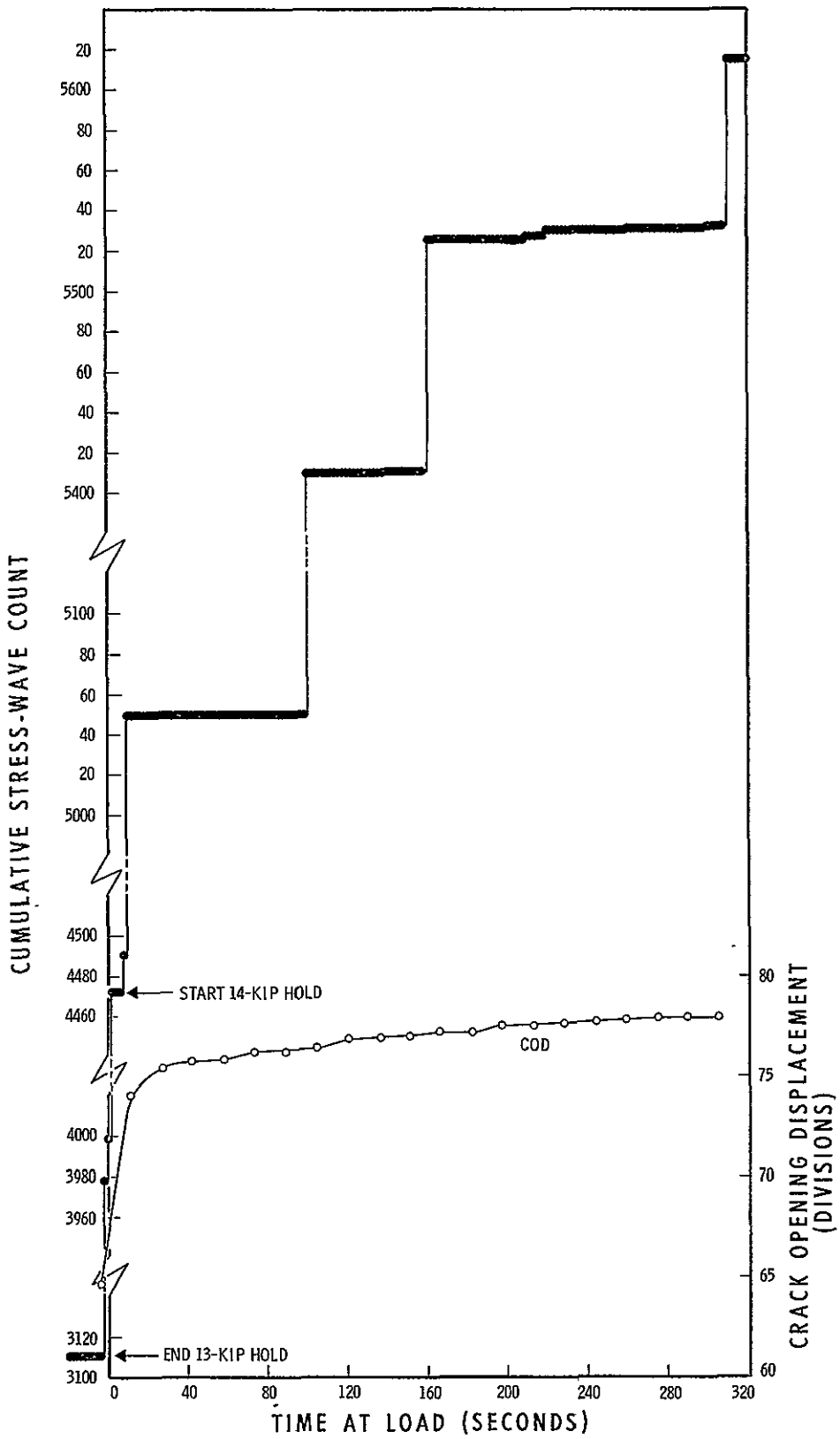

Figure 17. Cumulative Stress Wave Count and COD vs Time, Specimen No. 5, A302B Steel, Hydrogenated and Held at 14 Kips in Air

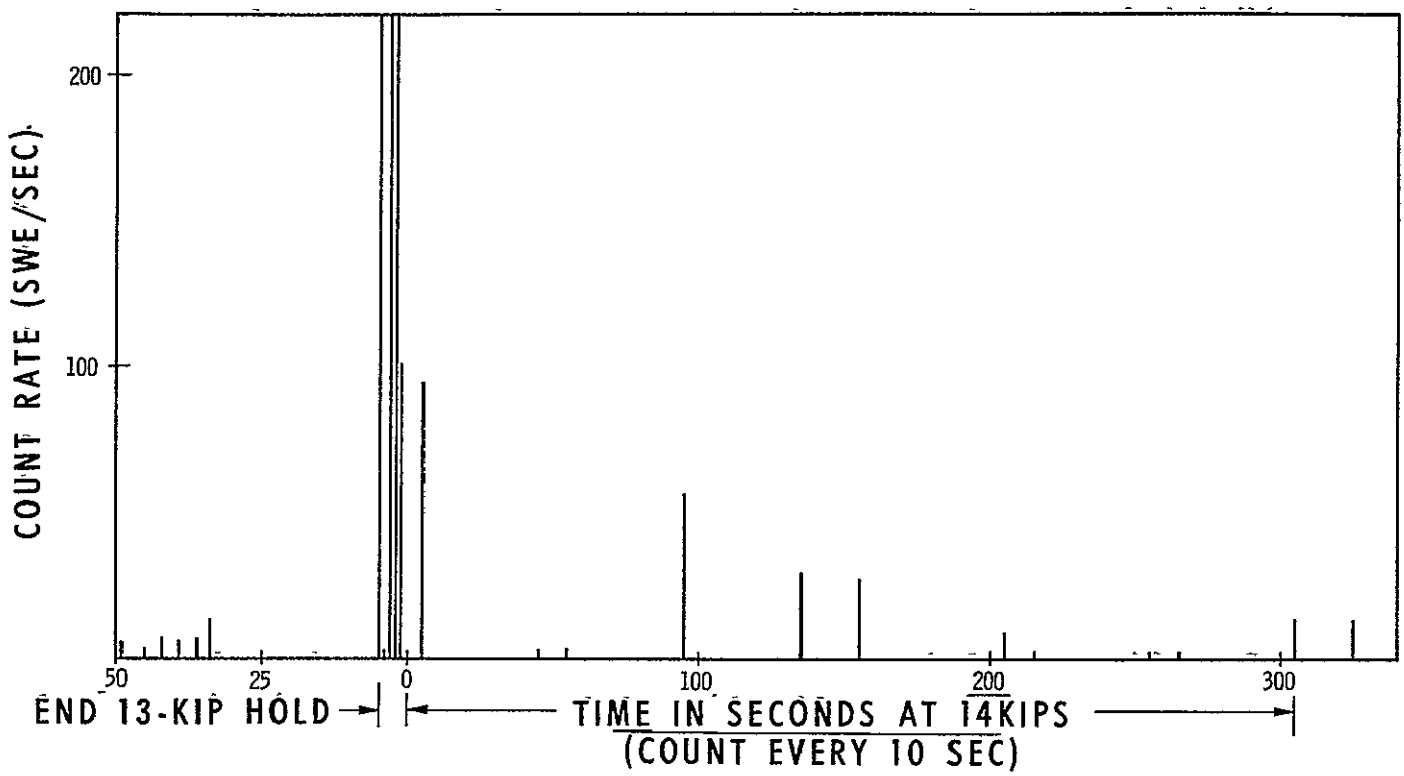

Figure 18. Stress Wave Count Rate vs Time - Specimen No. 5, A302B Steel, Hydrogenated and Tested in Air

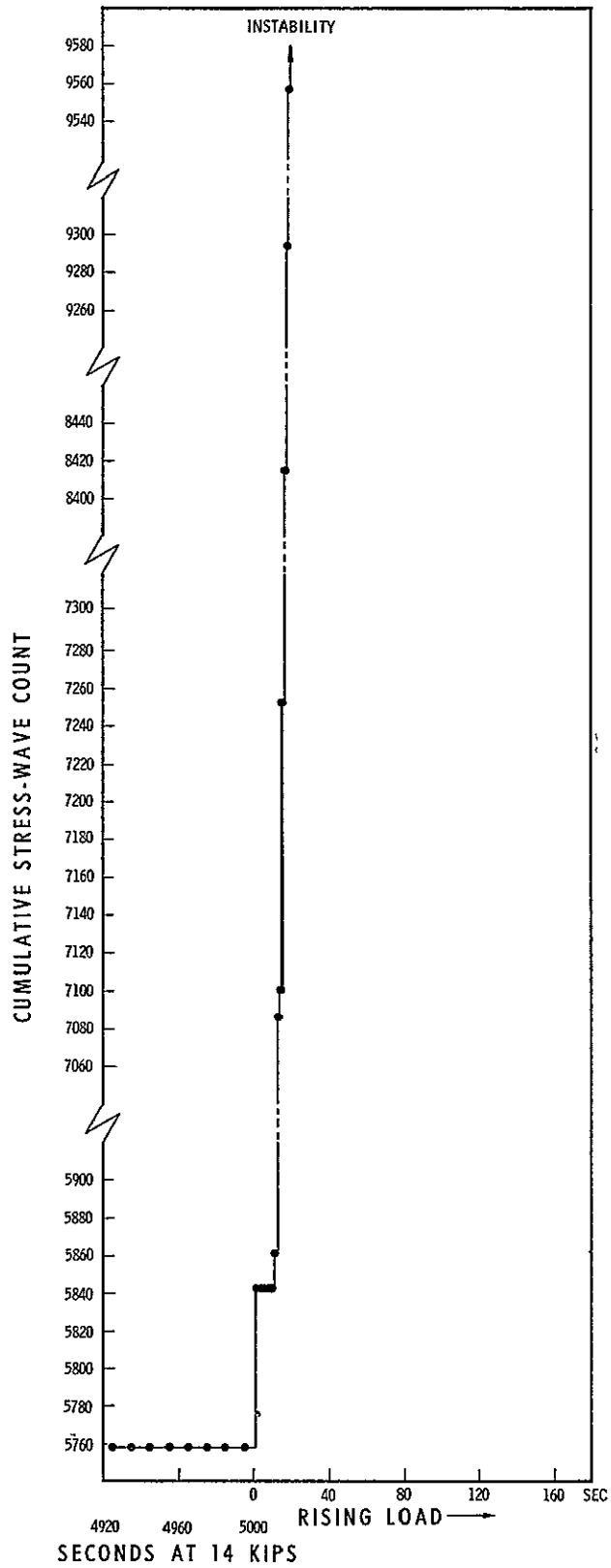

Figure 19. Cumulative Stress Wave Count vs Time, Specimen No. 5, A302B Steel, Hydrogenated and Tested in Air

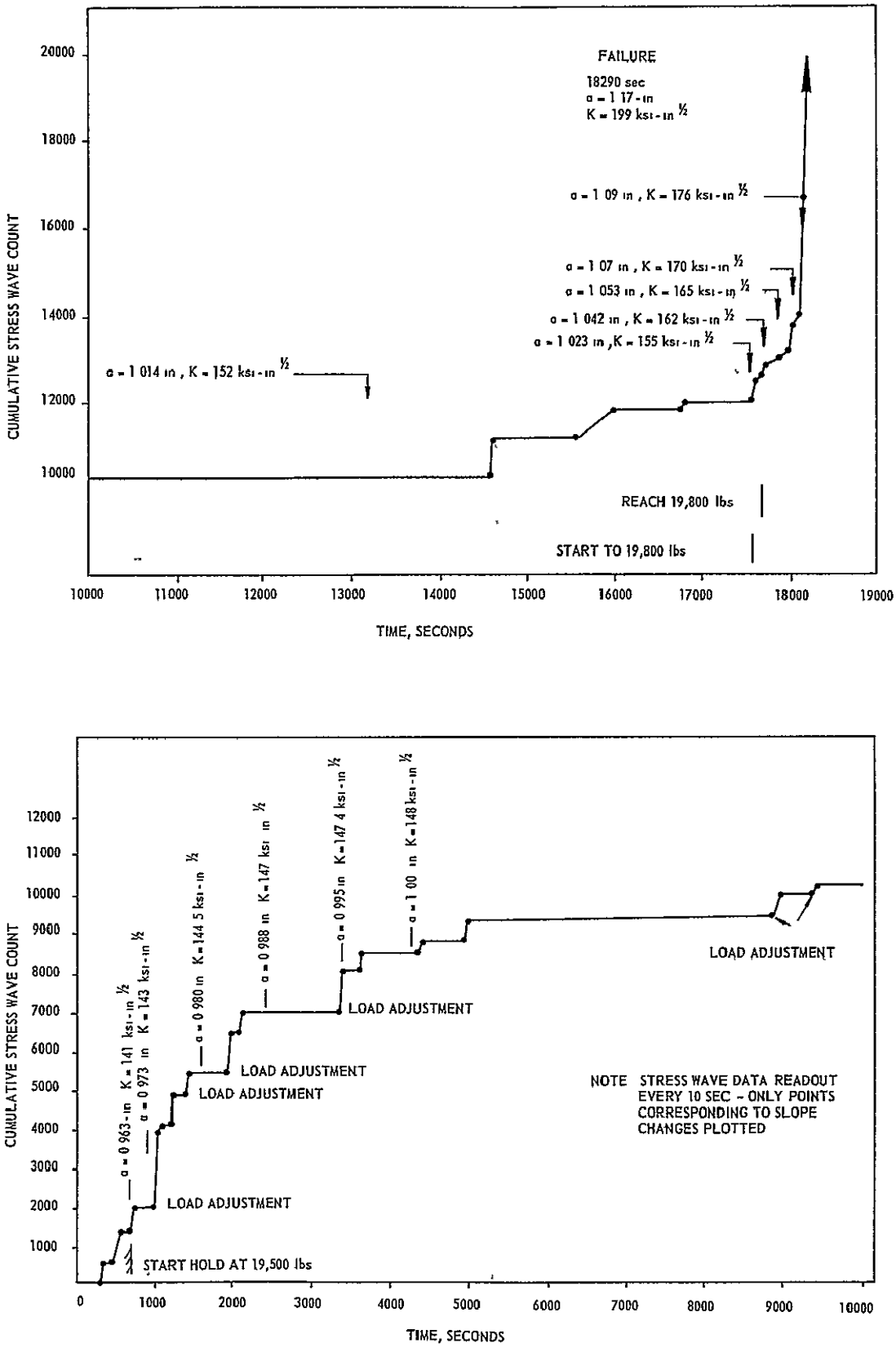

Figure 20. Cumulative Stress Wave Count vs Time, Specimen No. 6, A302B Steel, Hydrogenated and Tested in Air

IV, C, Bend Tests in Air With Deliberate Addition of Hydrogen (cont.)

As indicated in Figure 20, the increase in crack length during the initial period of hold at 19,500 lb resulted in an increase in the applied stress intensity and was accompanied by significant stress-wave-emission activity. To maintain the desired load, it was also necessary to make frequent load adjustments at the start of hold. During the first 3600 sec, the effective crack length increased from approximately 0.963 to 1.000 in, and was accompanied by about 7000 SWE. As indicated in Figure 20, the majority of the SWE activity and increase in crack length occurred during the first 3000 sec of the hold at 19,500 lb. After this period, both the stress-wave-emission activity and rate of increase in crack length gradually decreased. For example, during the entire period from 5000 to 17,600 sec when the load was increased to 19,800 lb, the apparent crack length and SWE count increased by only approximately 0.020 in. and 2500, respectively.

After approximately 17,000 sec at 19,500 lb, the load was increased to 19,800 lb and specimen failure occurred after approximately 600 sec at 19,800 lb. The load was maintained for this period; however, it was apparent from both the SWE and COD gage data that the crack was extending and specimen failure would occur without a further increase in load, although it was necessary to continually adjust the tensile machine to maintain the desired load. The failure stress intensity approximated 199 ksi-in.$^{1/2}$; however, technically, the onset of instability occurred after starting to increase the load at approximately 153 ksi-in.$^{1/2}$.

Specimen 7 was also hydrogenated, baked at 300°F for 3 hr, and tested in air. Figure 21 is a detailed plot of the SWAT data (electronic counter print-out every second) indicating crack growth of a discontinuous nature starting at 2400-lb load. Note the periods of dormancy (no increase in SWE count) interspersed with abrupt increases in count, indicating discontinuous crack growth. Note also that there was little or no evidence of continuous stress-wave emission until the load (stress intensity level) was high, approaching failure.

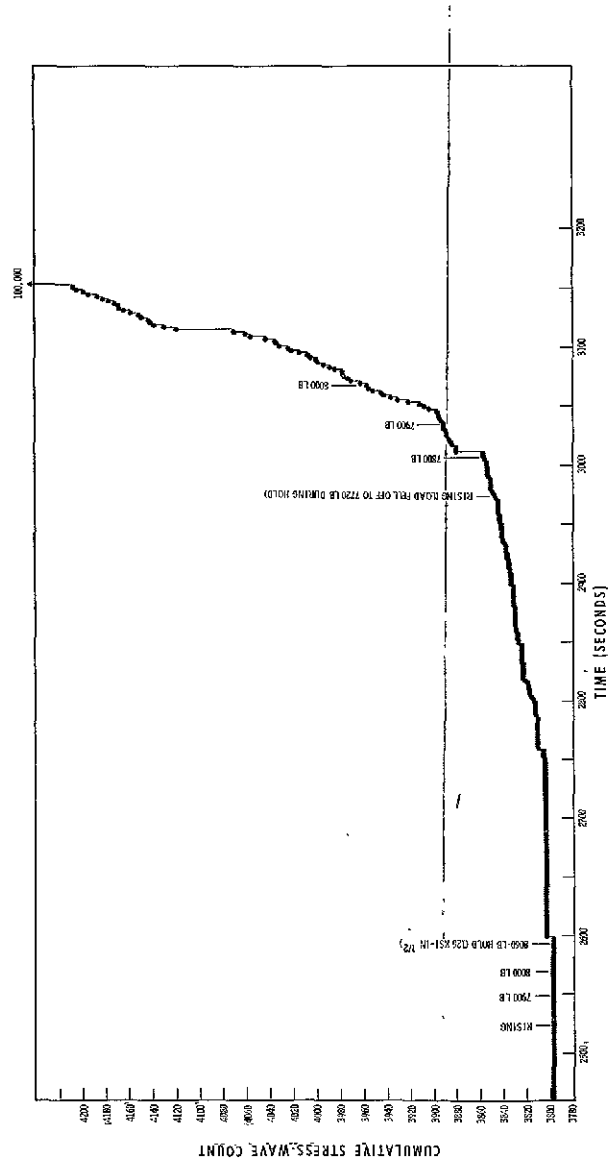

FOLDOUT FRAME 1

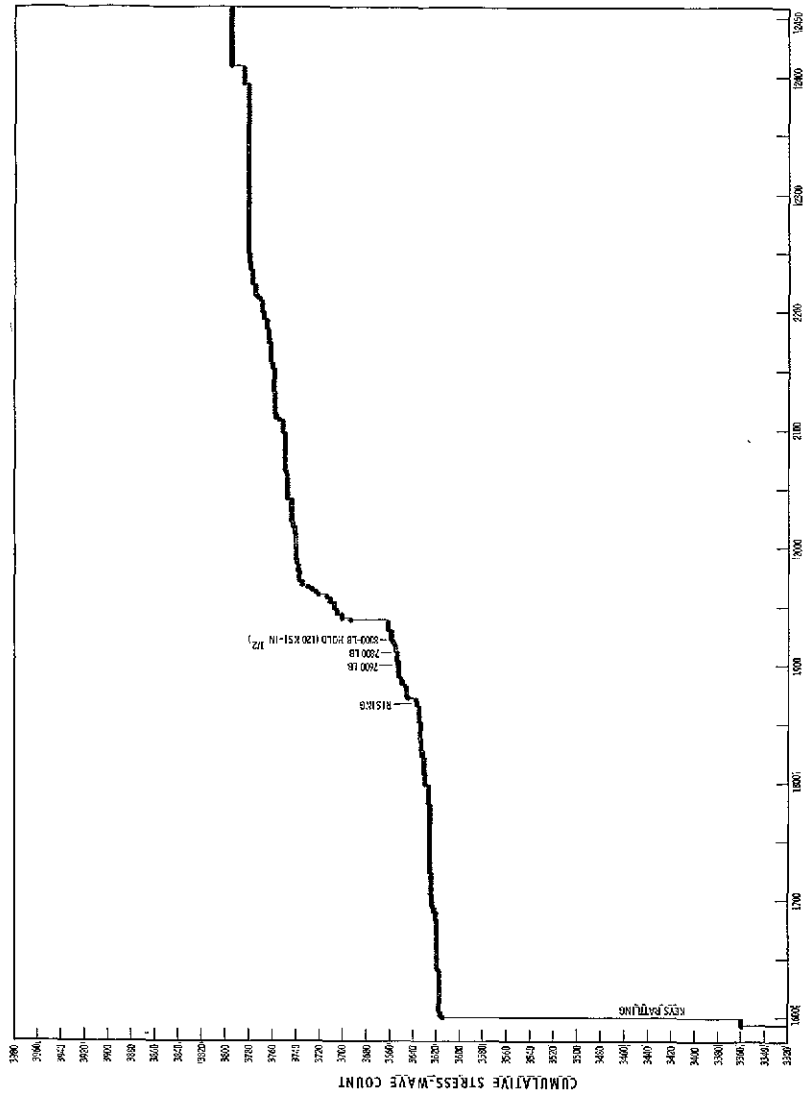

FOLDOUT FRAME 2

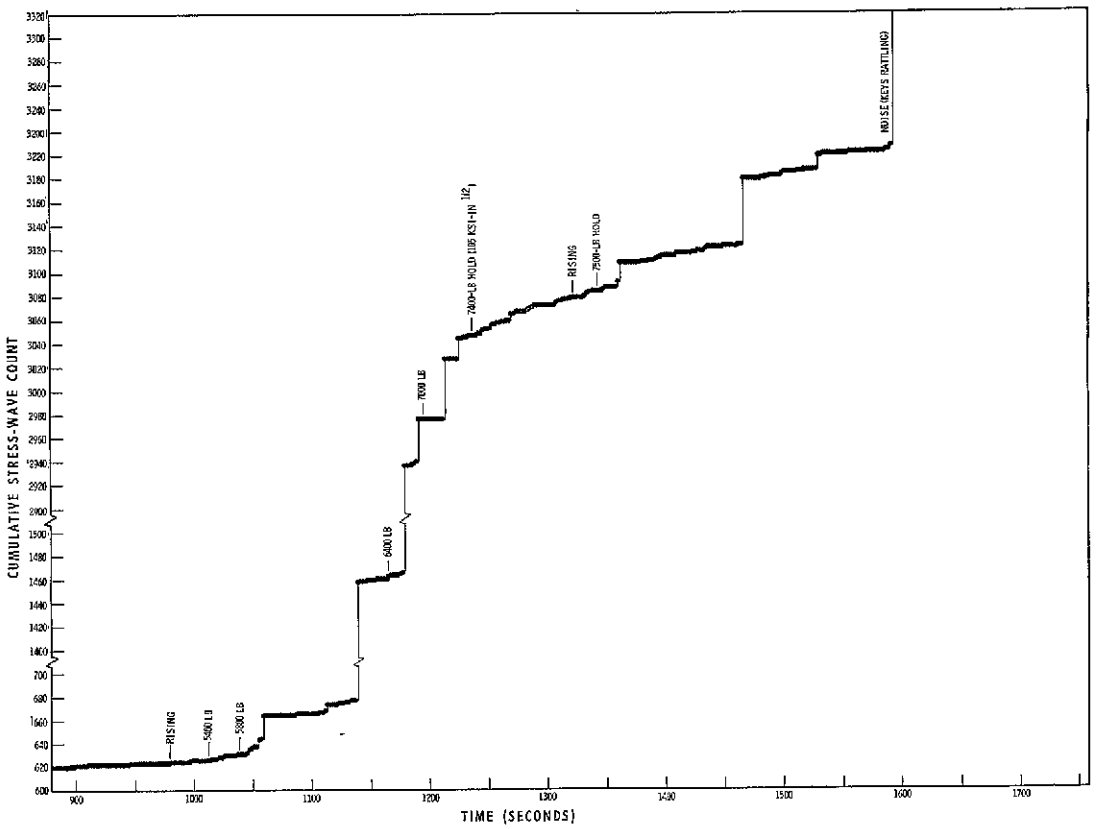

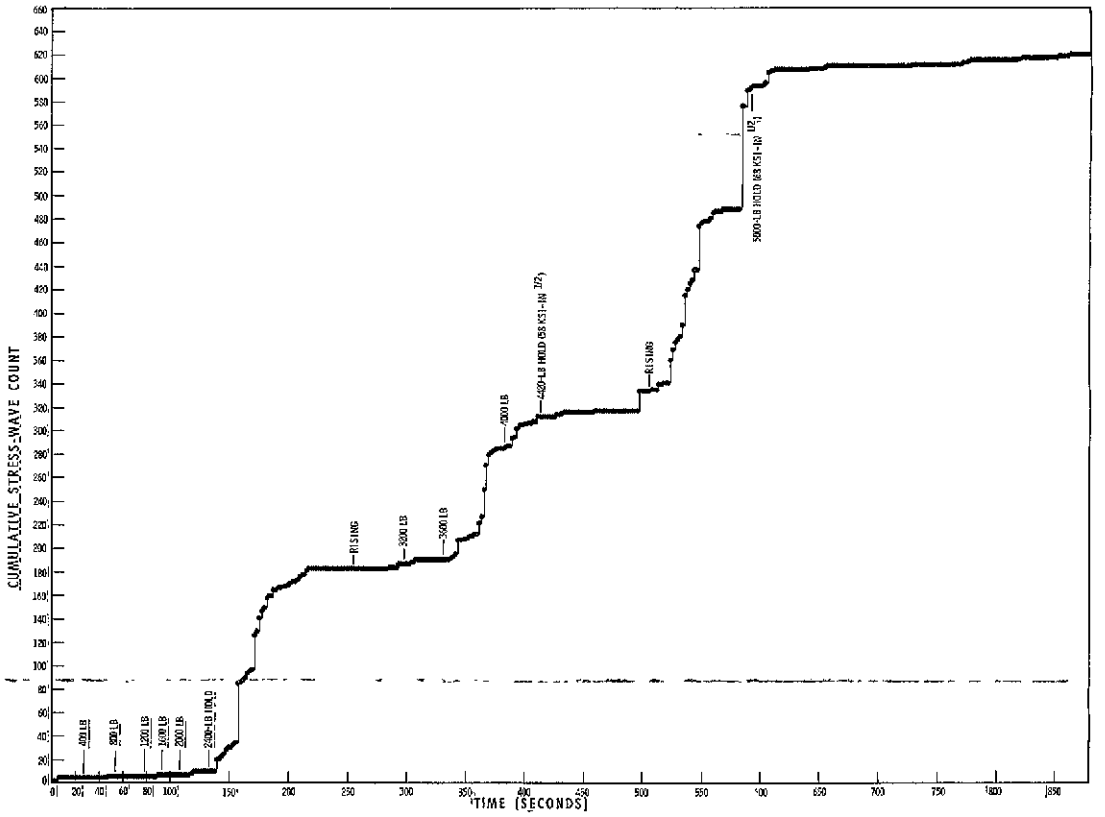

Figure 21. Cumulative Stress Wave Count vs Time, Specimen No. 7, A302B Steel, Hydrogenated and Tested in Air

IV, C, Bend Tests in Air With Deliberate Addition of Hydrogen (cont.)

Figure 22 presents the SWE data from a hydrogenated bend specimen (No. 8) tested in air. The load was increased continuously to 9800 lb (70 ksi-in.$^{1/2}$) where there was a short hold (approximately 400 sec). Note the discontinuous crack growth followed by a short period of continuous emission (less than 45° slope). The load was then raised to 14,800 lb (109 ksi-in.$^{1/2}$) and held for approximately 400 sec. Again, there were jumps in the SWE cumulative count, but this time interspersed with continuous emission. The SWAT system employed for this test corresponded to that employed for the background measurements at Kennedy Space Flight Center and shown in Figure 8; only one channel was employed, viz,

Endevco 2213 — Amplifier 100X — Amplifier 100X — Band-Pass Filter 20 to 50 Kcps

The continuous stress-wave emission observed during hold at the higher stress-intensity level in this specimen was not observed in the other hydrogenated specimens tested in air. The primary purpose of this test (Specimen 8) was to record SWE data for subsequent playback and analysis to determine the amplitude of burst-type stress-wave emissions associated with fracture in Type A302B steel. These analyses were performed using the instrumentation shown in Figures 7 and 8, with the following results which are discussed in more detail in conjunction with the results of the background measurements performed at Kennedy Space Flight Center (Section V).

Maximum SWE Amplitude - 3.9×10^{-3}g

Minimum SWE Amplitude - 1.2×10^{-3}g

Average SWE Amplitude - 2.2×10^{-3}g

Laboratory Background - 1.1×10^{-3}g

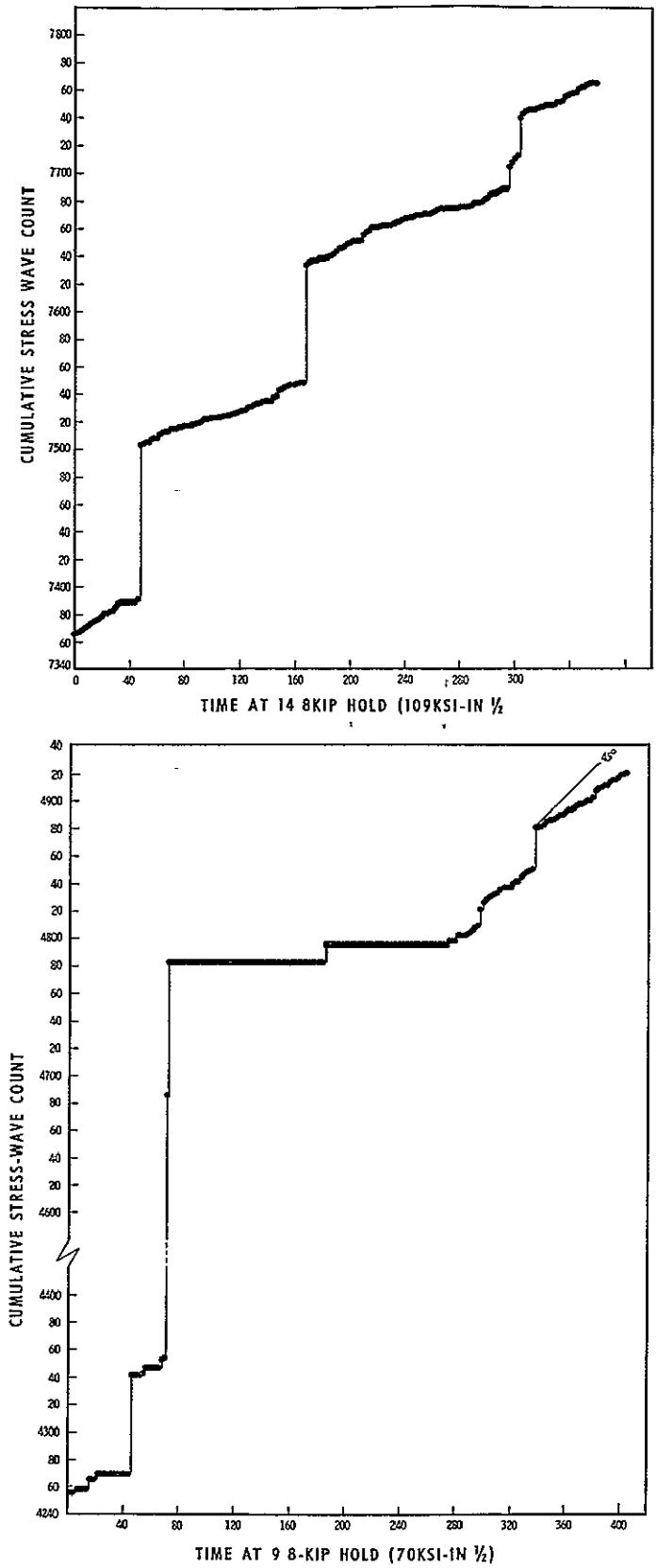

Figure 22. Cumulative Stress Wave Count vs Time, Specimen No. 8, A302B Steel, Hydrogenated and Tested in Air

IV, Laboratory Test Results and Discussion (cont.)

D. BEND TESTS IN 3% NaCl-WATER WITH DELIBERATE ADDITION OF HYDROGEN

Specimen 9 was hydrogenated, baked, and tested in 80°F water. The electronic counter indicated continuous stress-wave emission interspersed with abrupt increases in count, indicating occasional crack jumps. Figure 23 shows the details of stress-wave emission that occurred during both rising load and holding load. The crack length determined from the COD chart at selected loads is also shown. Note from the SWE data that there were no periods of dormancy and the slope of the plot of cumulative count versus time indicated moderately rapid, continuous crack growth such as might occur with electrochemical dissolution at the crack tip. The COD gage data shown in Figure 23 also indicate crack extension; however, the actual amount appears to be quite small (<0.1 in.) which would be consistent with the relatively small number of stress-wave emissions detected even at the high system sensitivity employed. The dramatic difference between the behavior in Figures 21 and 23 for hydrogenated material tested in air (Figure 21) and water (Figure 23) indicates that hydrogen and 3% sodium chloride solution, acting together, have a greater total effect than the sum of their individual effects; i.e., working together they appear to have produced a synergism.

E. WOL TESTS

Because of the possible significance of the synergistic effect noted above on the life of the hydrogen pressure vessels at Kennedy Space Flight Center, additional testing was performed using hydrogenated WOL specimens cut from the fractured bend specimens. The first WOL specimen was initially loaded to 3650 lb (50 ksi-in.$^{1/2}$) and then placed in 3% NaCl solution (notch immersed). There was 30 min of essentially continuous stress-wave emission (recorder started approximately 5 min after loading the specimen). Subsequently, there was one sizable jump in the SWE cumulative count after

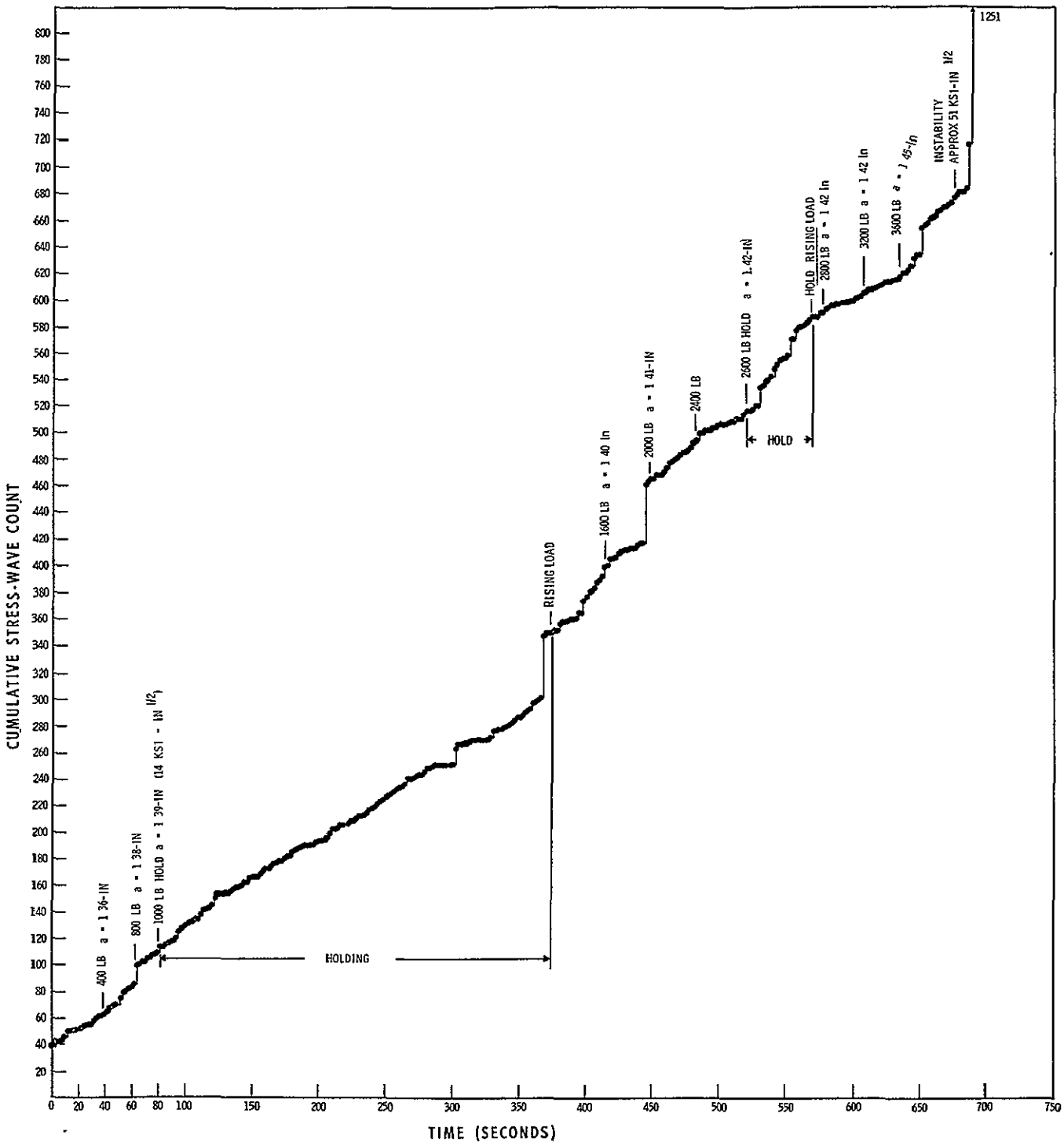

Figure 23. Cumulative Stress Wave Count vs Time, Specimen No. 9, A302B Steel, Hydrogenated and Tested in 3% NaCl-Water Environment

approximately 3 hr 40 min. Then, 3 hr 20 min later several jumps occurred followed by 8 hr 20 min of stress-wave activity. After this, the crack was dormant (total test time 17 hr 25 min). These data are shown in Figure 24. The load was then increased slightly (torque was increased from 200 to 255 in.-lb); an additional 1-1/2 hr in 3% NaCl solution produced no significant increase in the cumulative stress-wave count. The reason for this apparently anomalous behavior was not determined although it may result from a blunting effect at the crack tip produced during the initial hold period.

The fatigue crack was then extended (approximately 0.05 in.) in tension-tension fatigue and the specimen reloaded to approximately 51 ksi-in.$^{1/2}$. Stress-wave emission started almost immediately (dashed curve in Figure 24). After approximately 3 hr of discontinuous activity, the periods of dormancy tended to increase, interspersed with relatively small jumps (as counted over 10-sec intervals). The results of the initial loading and the reloading are shown in Figure 24; note that there was appreciably lower cumulative count in the reloaded specimen as compared with the initial loading for a comparable period of test.

A second hydrogenated WOL specimen was then tested in air at 50 ksi-in.$^{1/2}$; there were stress waves initially (creep), but then very little activity over the remaining 35-hr test period. After the first hour, the count increased from approximately 150 to only 280 in the final 34 hr of test. Figure 25 shows the long periods of dormancy punctuated by occasional 1-count increases. This is in marked contrast to the results obtained from the hydrogenated WOL specimens tested in 3% NaCl solution and the bend-test findings of a synergistic effect were confirmed.

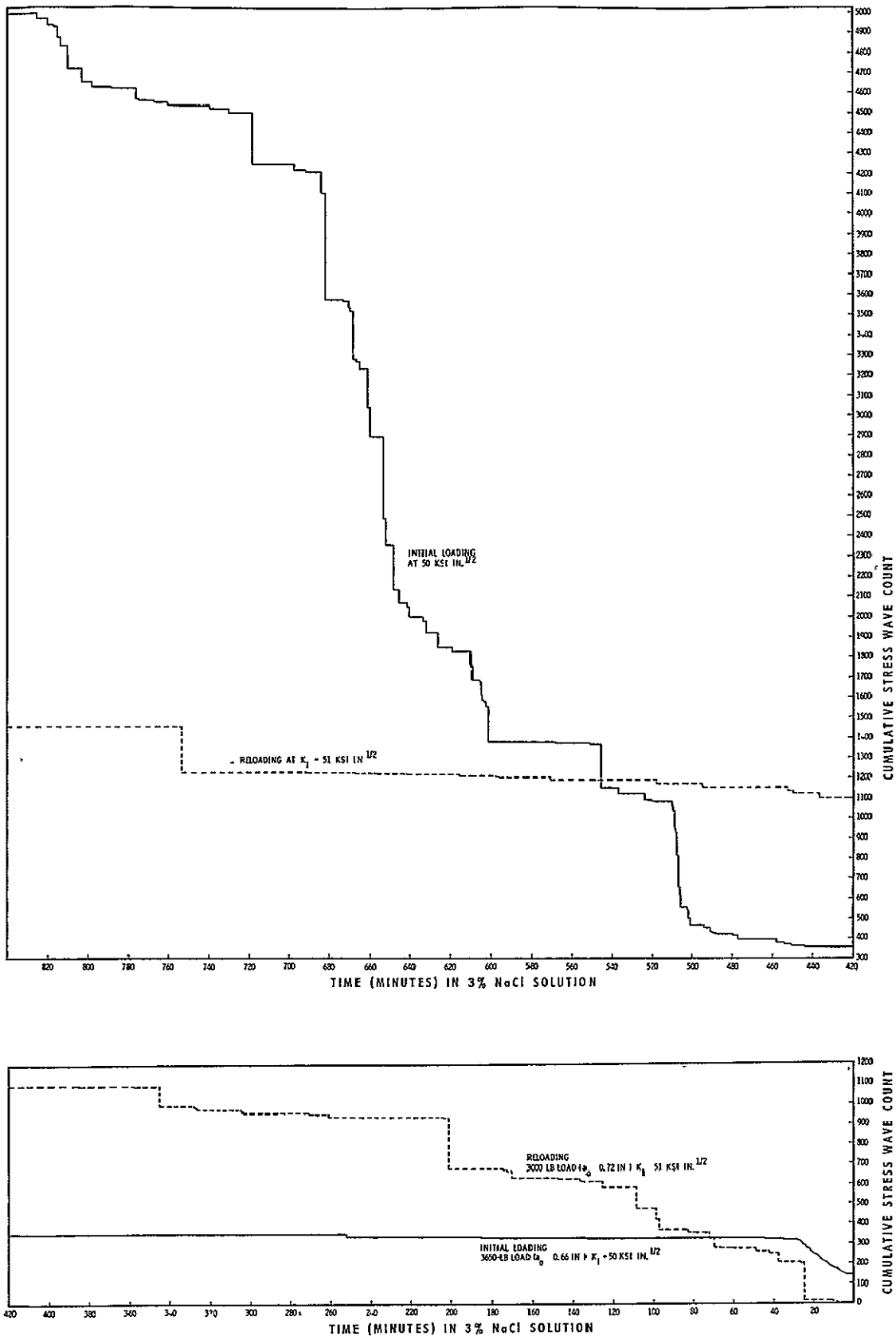

Figure 24. Cumulative Stress Wave Count vs Time at Hold, WOL Specimen No. 1, A302B Steel, Hydrogenated and Tested in 3% NaCl-Water Environment

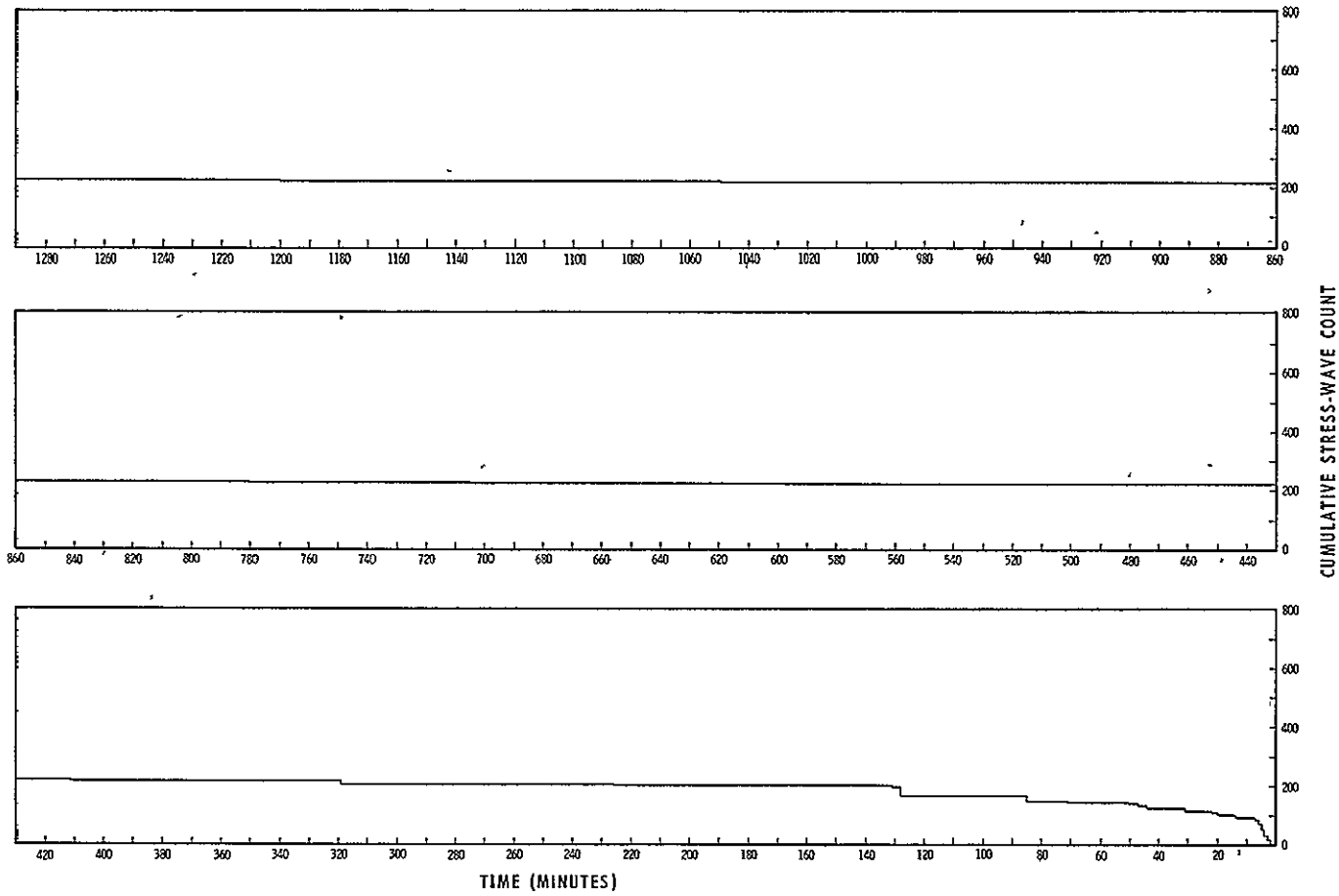

Figure 25. Cumulative Stress Wave Count vs Time at Hold, WOL Specimen No. 2, A302B Steel, Hydrogenated and Tested in Air

IV, Laboratory Test Results and Discussion (cont.)

F. DISCUSSION

1. Material-Environment Consideration

The Type A302B steel supplied for evaluation exhibited a very high level of fracture toughness. Although "quantitative" plane-strain fracture toughness measurements were not possible because of the large specimen size required, the K_Q value associated with failure approximated 135 ksi-in.$^{1/2}$. This material was also found resistant to environmentally induced failure in that the rate of crack growth of a prior flaw at applied stress-intensity factors as high as 90% of the K_Q value appeared to be very low. This effect was observed for unhydrogenated material tested in air and a 3% NaCl-water environment, and hydrogenated material tested in an air environment. However, the hydrogenated specimens tested in 3% NaCl-water environment had a much faster rate of subcritical crack growth in comparison to the other test conditions indicating a synergistic effect due to the combination of sea water and hydrogen in interstitial solid solution. This synergistic effect indicates that the Type A302B steel hydrogen storage tanks in the Kennedy Space Flight Center environment may have limited life as the result of subcritical crack growth if subjected to the same combination of stress and environmental factors.

The WOL test results tended to confirm the possible synergism due to the combined effects of 3% NaCl-water and hydrogen in interstitial solid solution. Marked SWE activity was observed when the hydrogenated specimens were immersed in the salt water; whereas in an air environment after the initial period at hold when a creep phenomenon was observed, there was essentially no stress-wave emission. The fact that failure was not produced on holding (in contradiction to the bend tests) can be explained by the fact that the WOL test as performed in this program, is a self-arresting test, because

the occurrence of crack growth results in a reduction in the applied load. Conversely, in the bend tests, the load was constantly applied as the crack extended and eventually resulted in specimen failure.

2. Stress-Wave-Emission Characterization

Detectable stress-wave emissions, although of small amplitude (<0.01g), were observed to be associated with crack growth in Type A302B steel. Under all test conditions, the stress-wave emissions were observed both during rising load and when failure (instability) was imminent. During hold, various SWE characteristics, depending on the test conditions, were observed. When tested in the hydrogenated condition in an air environment, a creep phenomenon evidenced by increasing count of SWE and an accompanying increase in apparent crack size was observed. With time at hold and at applied stress-intensity levels less than critical, the creep phenomenon eventually stopped, as did the occurrence of stress-wave emissions. Unhydrogenated material tested in the 3% NaCl-water environment produced continuous stress-wave emission punctuated by abrupt increases in SWE count. This behavior indicates both continuous, very small increments of crack extension, with larger crack jumps corresponding to the abrupt increases in SWE count. Continuous incremental crack extension characterized by continuous SWE interspersed with abrupt increases in SWE count, indicating occasional crack jumps, was also observed in testing hydrogenated material in a 3% NaCl-water environment.

In all instances, when failure (instability) occurred, both the amplitude and rate of stress-wave emission increased and could be employed as a precursor of the onset of instability; however, even when failure was approached, the SWE amplitude was small (<0.1g). In the other instances where failure was not produced, evidence of crack extension (although very small in some instances) was observed on the specimen fracture face. Once evidence of

IV, F, Discussion (cont.)

crack growth was observed (by SWE or COD), it is obvious that failure would eventually occur (assuming a constantly applied load), although depending on the initial flaw size and subcritical growth rate, the time to failure may be very long. In actual practice the SWE data could be employed (1) to locate the propagating flaw, (2) to monitor its occurrence, and (3) as a basis for terminating service so that repairs could be made before failure. The stress-wave emissions associated with crack growth during rising load or increasing stress intensity, and the "creep" phenomenon during the initial part of hold can be employed for this purpose.

V. BACKGROUND MEASUREMENTS AND ASSOCIATED LABORATORY TESTS

A. BACKGROUND MEASUREMENTS AT KENNEDY SPACE FLIGHT CENTER

Background noise measurements were made at two locations: the VAB Bottle Field and Pad A at the Kennedy Space Flight Center. The data were tape recorded and, in addition to general background noise, included tank blowdown and repressurization periods. The instrumentation for this purpose is shown schematically in Figure 8; analysis of the data was performed by playback onto an oscillograph and comparison with the SWE-crack growth data obtained during the laboratory testing of bend specimens.

The analysis of the signal amplitude data for tests at Cape Kennedy is indicated below:

1. Pad A Bottle Field

		Signal Amplitude
a.	Quiescent Background	
	Filter at 20 Kcps - 50 Kcps Band Pass	- 9.9×10^{-5} g's
	Filter at 200 cps - 32 Kcps Band Pass	- 1.87×10^{-4} g's
b.	Tank Blowdown	- System Saturation (> 1.1g peak to peak)
c.	Tank Repressurization	- System Saturation (> 1.1g peak to peak)

2. VAB Bottle Field

a.	Quiescent Background	- 2.2×10^{-4} g's

V, A, Background Measurements at Kennedy Space Flight Center (cont.)

		Signal Amplitude
b.	Tank Blowdown	- System Saturation (> 1.1g peak to peak)
c.	Tank Repressurization	- System Saturation (> 1.1g peak to peak)

Analysis of the tape-recorded data of bend tests at Aerojet indicates the following signal amplitude for "burst"-type stress-wave emissions associated with crack growth and fracture in Type A302B steel.

Maximum Amplitude	-	3.9×10^{-3} g
Minimum Amplitude	-	1.2×10^{-3} g
Average Amplitude	-	2.2×10^{-3} g
Laboratory Background	-	1.1×10^{-3} g

Thus, the amplitude of SWE associated with crack growth in A302B steel is approximately an order of magnitude larger than the background noise noted previously. Consequently, the above results show that it is possible to detect stress-wave emissions associated with fracture in A302B steel under the quiescent background conditions existing at the Kennedy Space Center. Difficulty is expected in detecting such flaw growth during tank blowdown and repressurization periods unless filtering can be employed to screen out the noise associated with these periods. However, the blowdown and repressurization periods are of very short duration and the materials behavior observed in this program indicated that considerable prefailure crack extension would be expected from any flaw of a size expected to be present in these pressure vessels. Also, immediately on reaching load, a "creep" phenomenon evidenced by an extension in apparent crack length and accompanied by detectable stress-wave emission was observed. Consequently, even if noise associated with blowdown and

repressurization cannot be effectively filtered out, significant flaw growth and/or creep could still be detected and tank depressurization accomplished prior to catastrophic failure assuming a capability for such depressurization exists at these locations.

B. LABORATORY SIGNAL ATTENUATION EVALUATIONS

Subsequent to the background measurements at the Kennedy Space Flight Center and the bend tests at Aerojet, two series of tests were made at Aerojet using a section of pipe and plate, both of SAE 4130 steel alloy. The purpose of these tests was to determine the coefficient of signal attenuation which in conjunction with the previous test data, could be used to establish the sensor spacing which would insure detection of SWE associated with crack growth in the pressure vessels at the Kennedy Space Flight Center.

In these tests, a constant pulse was imparted to the specimen by a Tektronix 115 Pulse Generator using a Clevite PZT-5 Crystal (2.125 in. dia and 0.250 in. thick). The piezoelectric crystal was mounted on a small aluminum block, which in turn was adhered to the surface of the specimen. The signal was received by a 2217-E-Endevco accelerometer placed at various distances from the pulser. The pulse used was 10 n-sec rise and fall time, with a duration of 20 microsec at an amplitude of 1.2v.

1. Pipe Tests

A SAE 4130 steel pipe (8-5/8 in. OD, 7-1/8 in. ID, and 22 ft 10-7/8 in. long) was used as specimen for this test series. The pulser was mounted normal to the external surface of the pipe as close as possible to the edge. The accelerometer (2217-E-Endevco) was successively placed on the pipe

V, B, Laboratory Signal Attenuation Evalutions (cont.)

surface at positions 1 to 8 that were at 4, 6, 8, 10, 12, 14, 16 and 20 ft from the pulser. The signal received by the accelerometer was displayed on a Tektronix 422 oscilloscope. Typical signals are shown in Figure 26.

The velocities of the compressional and shear waves in steel are

$$v_c = \sqrt{\frac{E(1-\mu)}{\rho(1+\mu)\ (1-2\mu)}} = \sqrt{\frac{29 \times 10^6\ (1-0.30) \times 386}{0.283\ (1+0.30)\ (1-0.60)}} = 227{,}000 \text{ in./sec}$$

$$v_s = \sqrt{\frac{E}{2\ (1+\mu)\ \rho}} = \sqrt{\frac{29 \times 10^6 \times 386}{2\ (1+0.30) \times 0.283}} = 123{,}000 \text{ in./sec}$$

where E = Young's Modulus, μ = Poisson's Ratio and ρ = density. The times of arrival of these waves at the computed velocities are indicated on the oscilloscope photos shown in Figure 26. The point of shear wave arrival (T_s) coincides in most of the photos to a distinct change of pattern in the trace. The arrival of the compressional wave is difficult to determine accurately because the amplitude of this wave attenuates very fast with distance.

A visual comparison of the curves shows that Figure 26a, representing the signal received 4 ft from the impulse, indicates a perfectly detectable arrival of the compressional wave; conversely, Figure 26h (at 20 ft from the impulse) shows the visually detectable arrival of a wave almost at the computed arrival of the shear wave. This is due to the fact that the amplitude of the first cycles of the compressional wave have become essentially imperceptible at a distance of 20 ft from the pulse. An attempt to determine signal arrival time by visual inspection only of the traces in Figure 26 would result in the wave velocities indicated in Table III. The computed arrival times of the compressional and shear waves are shown in Table IV. If an integration of the positive portions of the cycles comprised in 200 μ sec after arrival of the

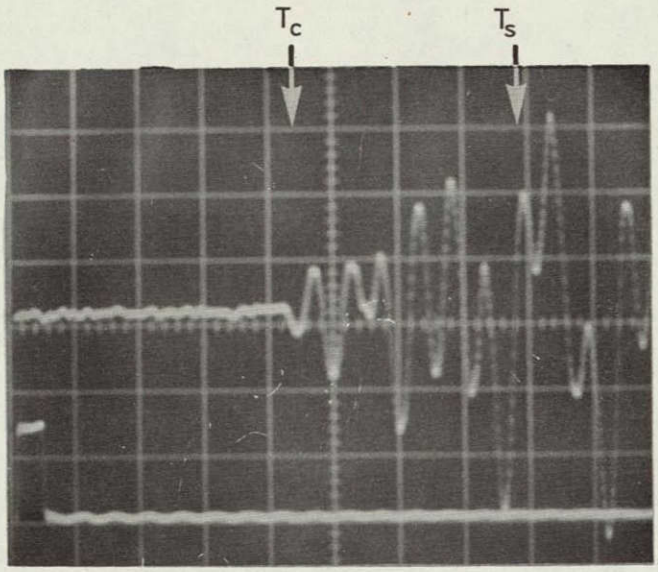

VERTICAL SCALE 1 DIV = 0.1 V
HORIZONTAL SCALE 1 DIV = 50 μ SEC

a. 4 FT FROM PULSER

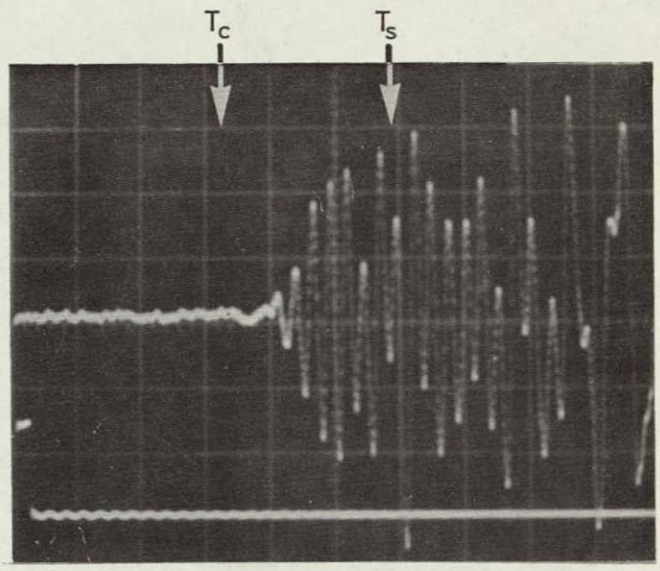

VERTICAL SCALE 1 DIV = 0.1 V
HORIZONTAL SCALE 1 DIV = 100 μ SEC

b. 6 FEET FROM PULSER

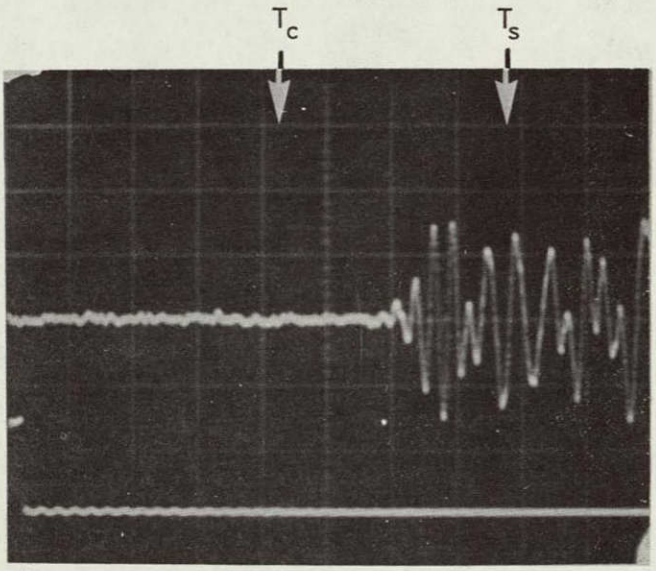

VERTICAL SCALE 1 DIV = 0.1 V
HORIZONTAL SCALE 1 DIV = 100 μ SEC

c. 8 FEET FROM PULSER

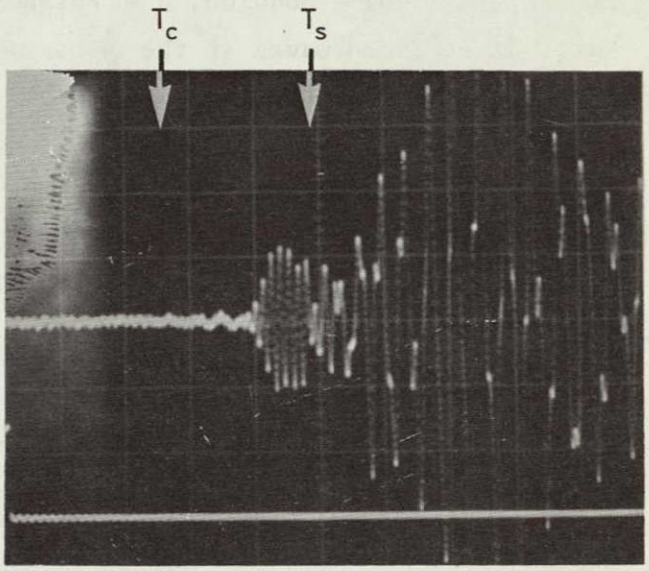

VERTICAL SCALE 1 DIV = 0.1 V
HORIZONTAL SCALE 1 DIV = 200 μ SEC

d. 10 FEET FROM PULSER

T_c = Arrival of Compressional Wave
T_s = Arrival of Shear Wave

Figure 26. Oscillograph Traces for Pipe Tests (Sheet 1 of 2)

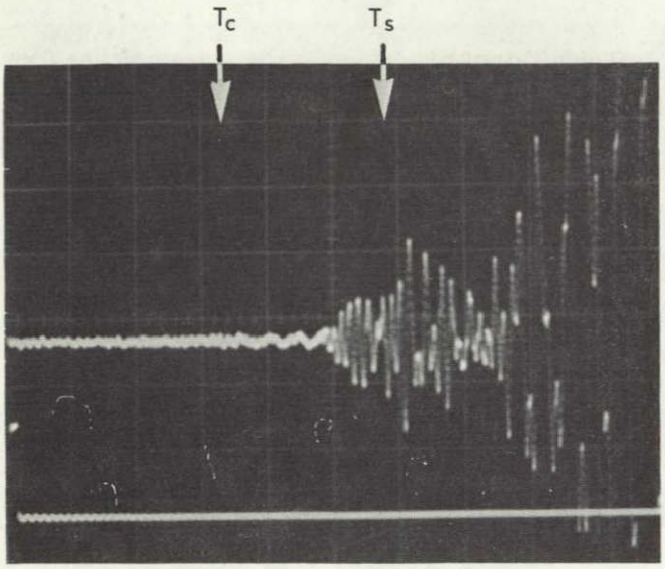

VERTICAL SCALE 1 DIV = 0.1 V
HORIZONTAL SCALE 1 DIV = 200μ SEC

e. 12 FEET FROM PULSER

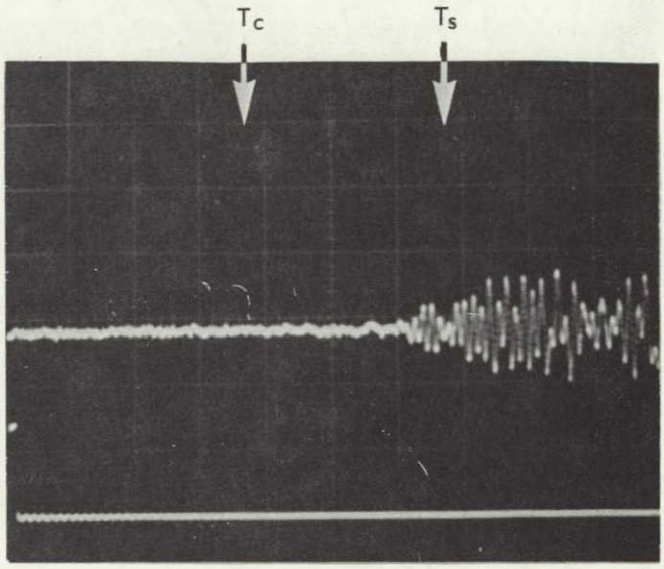

VERTICAL SCALE 1 DIV = 0.1 V
HORIZONTAL SCALE 1 DIV = 200 μ SEC

f. 14 FEET FROM PULSER

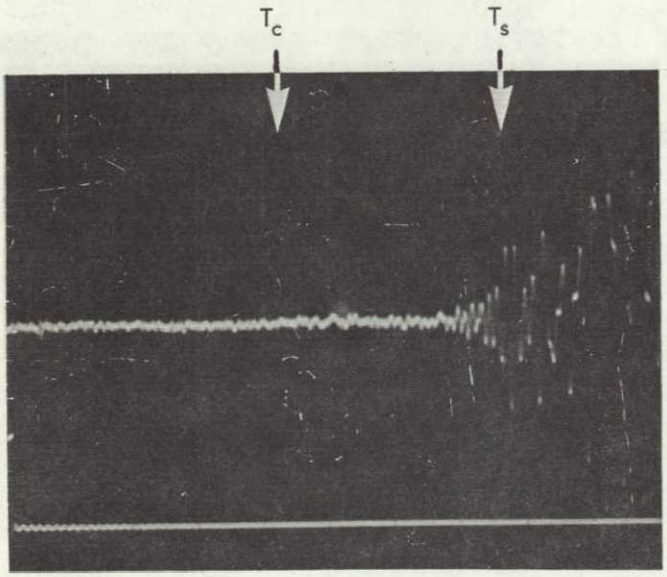

VERTICAL SCALE 1 DIV = 0.1 V
HORIZONTAL SCALE 1 DIV = 200 μ SEC

g. 16 FEET FROM PULSER

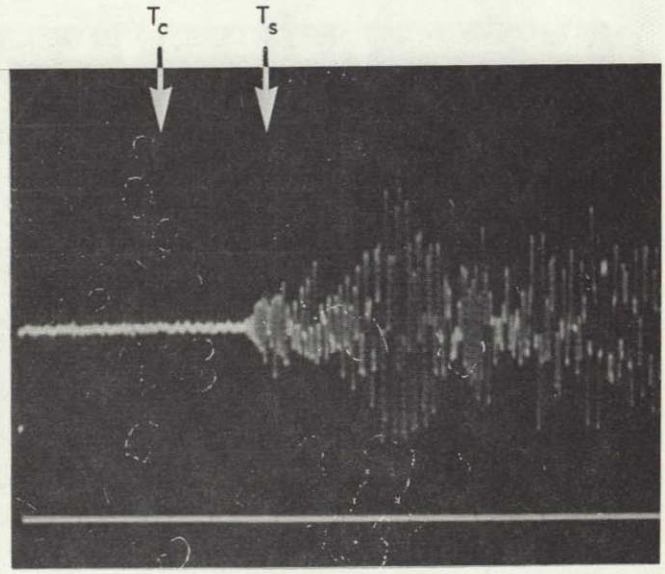

VERTICAL SCALE 1 DIV = 0.1 V
HORIZONTAL SCALE 1 DIV = 500 μ SEC

h. 20 FEET FROM PULSER

Figure 26. Oscillograph Traces for Pipe Tests (Sheet 2 of 2)

V, B, Laboratory Signal Attenuation Evaluations (cont.)

shear wave is performed, the average amplitudes determined in this manner become quite meaningful. These average amplitudes are shown in Table V.

TABLE III

WAVE VELOCITY BASED ON VISUAL ANALYSIS OF OSCILLOSCOPE TRACES - PIPE TESTS

Photo	Distance from Pulse ft	Distance from Pulse in.	Arrival Time, μsec	Velocities (ft/sec)
1	4	48	210	228,000
2	6	72	400	180,000
3	8	96	600	160,000
4	10	120	800	150,000
5	12	144	1000	144,000
6	14	168	1200	140,000
7	16	192	1400	137,000
8	20	240	1750	137,000

TABLE IV

COMPUTED ARRIVAL TIMES - PIPE TESTS

Photo	Distance from Pulse, in.	Compressional Wave Arrival Time μsec	Compressional Wave Arrival Time Osc. Div.	Shear Wave Arrival Time μsec	Shear Wave Arrival Time Osc. Div.
1	48	212	4.23	390	7.80
2	72	317	3.17	583	5.83
3	96	422	4.22	778	7.78
4	120	530	2.65	972	4.86
5	144	635	3.17	1163	5.81
6	168	740	3.70	1360	6.80
7	192	840	4.20	1545	7.71
8	240	1050	2.1	1930	3.87

V, B, Laboratory Signal Attenuation Evalutions (cont.)

TABLE V

SIGNAL AMPLITUDE VS DISTANCE - PIPE TESTS

Test	Distance from Pulser, in.	Average Signal Amplitude 200 μsec after Arrival of Comp. Wave, mv
1	48	230
2	72	145
3	96	85
4	120	60
5	144	45
6	168	28
7	192	22
8	240	18

The general equation for the amplitude attenuation curve is:

$$y = C \times e^{-\alpha x}$$

where y = amplitude at distance x, in volts

x = distance in inches from pulse source

C = amplitude of pulse in volts

α = attenuation factor

$$\text{or } {}_{1}{}_{n}y = {}_{1}{}_{n}C + (-\alpha x) = {}_{1}{}_{n}C - \alpha x \qquad \text{(Eq 4)}$$

To determine the values of C and α, the following statistical analysis was performed.

V, B, Laboratory Signal Attenuation Evaluations (cont.)

Test	Distance, in.	y, m v	$1_n y$	Y	Y^2	X	X^2	XY	$x.1_n y$
1	48	230	5.43	+1.42	2.010	-87	7,580	- 124	261
2	72	145	4.99	+0.98	0.960	-63	3,960	- 62	360
3	96	85	4.45	+0.44	0.194	-39	1,520	- 17	427
4	120	60	4.09	+0.08	0.006	-15	225	- 1	490
5	144	45	3.80	-0.21	0.044	+ 9	81	- 2	548
6	168	28	3.34	-0.67	0.450	+33	1,090	- 21	560
7	192	22	3.09	-0.92	0.847	+57	3,250	- 52	592
8	240	18	2.89	-1.12	1.250	+105	11,000	- 118	690

$\Sigma x = 1080$ $\Sigma 1_n y = 32.08$ $\Sigma Y^2 = 5.761$ $\Sigma X^2 = 28,706$ $\Sigma XY - 397$ $\Sigma x 1_n y = 3,928$

$$\bar{x} = \frac{1080}{8} = 135 \qquad \bar{1_n y} = \frac{32.08}{8} = 4.01$$

$$\alpha = \frac{\Sigma XY}{\Sigma_X 2} = -\frac{-397}{28.706} = 0.0138 \qquad 1_n C = \bar{1_n y} + \alpha\bar{x} =$$

$$= 4.01 + (.0138)(135) = 4.01 + 1.86 = 5.87$$

$$C = 355 \text{ mv}$$

It is now possible to compute the statistically corrected values of the signal amplitude, y, at the distances from the pulse where they were measured. The general formula will be:

$$1_n y = 5.87 - (0.0138) \cdot X$$

and the results are tabulated in Table VI. The computed value of pulse amplitude at source is found to be C = 355 mv. The values shown on Table VI are plotted in Figure 27, which graphically shows the signal attenuation as a function of distance from the pulse source.

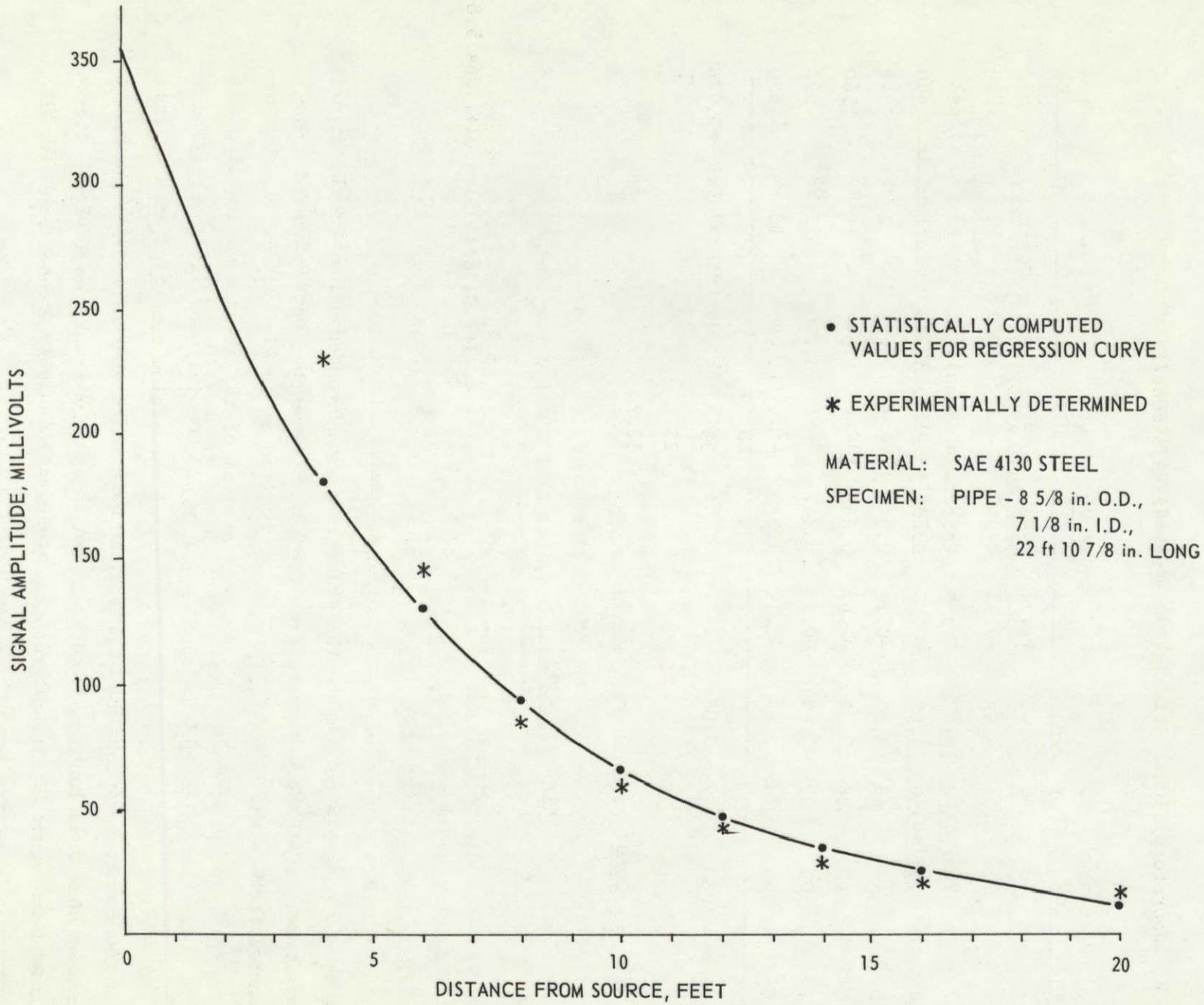

Figure 27. Signal Amplitude vs Distance - Pipe Tests

V, B, Laboratory Signal Attenuation Evaluations (cont.)

TABLE VI

STATISTICALLY CORRECTED VALUES OF SIGNAL AMPLITUDE - PIPE TESTS

Test	Distance from Pulse, in.	$\ln y$	Corrected Signal Amplitude (y), mv	Experimentally Determined Signal Amplitude (y), mv
1	48	5.21	182	230
2	72	4.88	130	145
3	96	4.55	95	85
4	120	4.21	67	60
5	144	3.88	48	45
6	168	3.55	35	28
7	192	3.22	25	22
8	240	2.55	12.7	18

2. Plate Tests

An SAE 4130 steel plate (73-1/2 in. long, 48-1/2 in. wide, and 3/4 in. thick) was used for this test series. The two diagonals were marked on the plate. The pulser was placed at the center of the plate and the receiver accelerometer was placed on one of the diagonals at locations spaced in increments of 6 in. from the center. The received signals were observed on the oscilloscope and photos were taken of these signals. Figure 28 shows oscillographs of the signals received at 6, 12, 18, 24, 30, 36, and 42 in. from the pulser. The times of arrival of the shear wave are also shown in Figure 28. The velocity used was v_s = 123,000 in./sec. An integration was performed of the positive positions of the cycles comprised in a 20 μsec interval after the arrival of the shear wave. The average amplitudes determined from these integrations are shown in Table VII. Only Tests 1 to 4 are used because reflection (from the plate edges) in Tests 5 to 8 obscured the

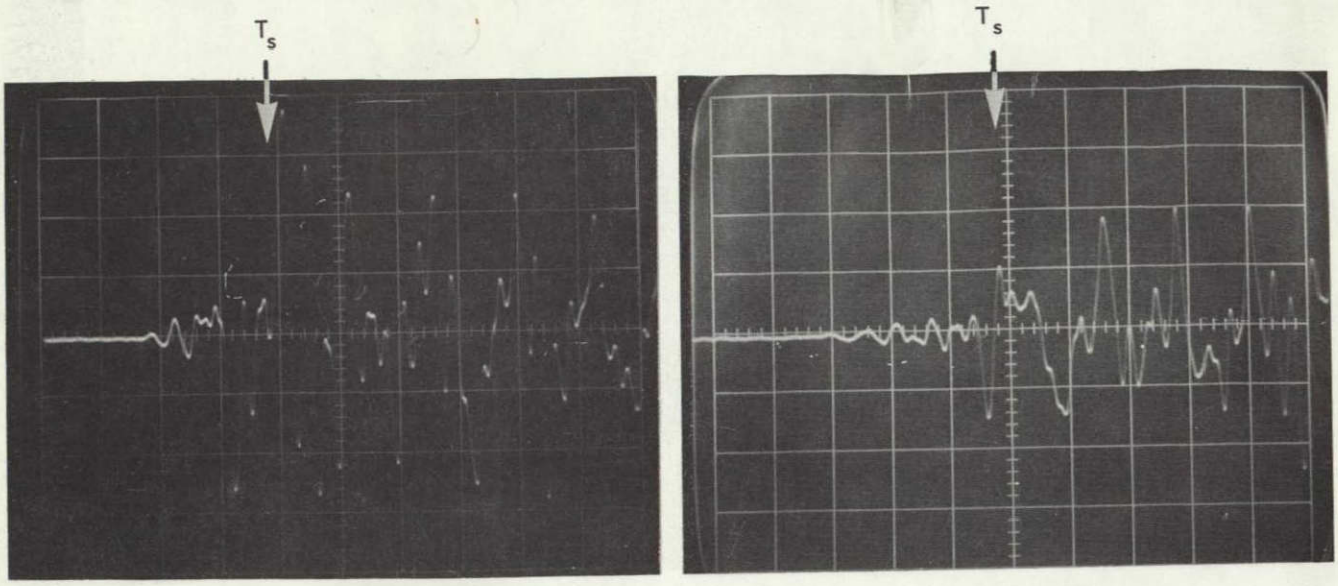

a. 6 INCHES FROM PULSER

b. 12 INCHES FROM PULSER

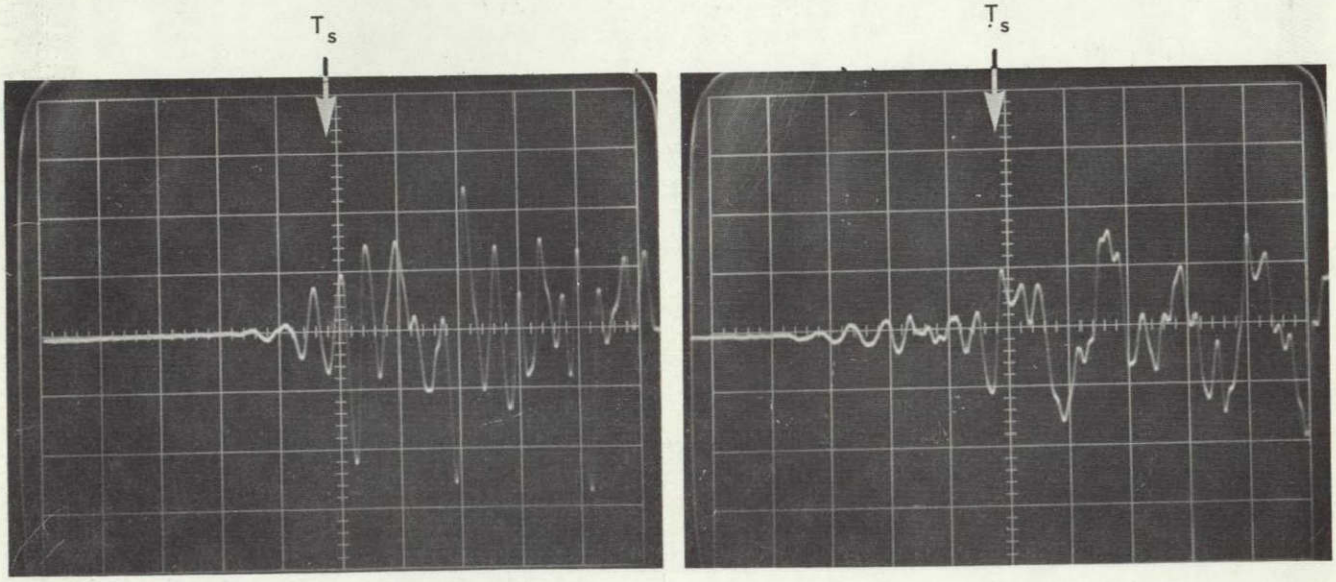

c. 18 INCHES FROM PULSER

d. 24 INCHES FROM PULSER

T_s = Arrival of Shear Wave
Vertical Scale 1 DIV = 0.1 Volt
Horizontal Scale 1 DIV = 20 μ Sec

Figure 28. Oscillograph Traces for Plate Tests (Sheet 1 of 2)

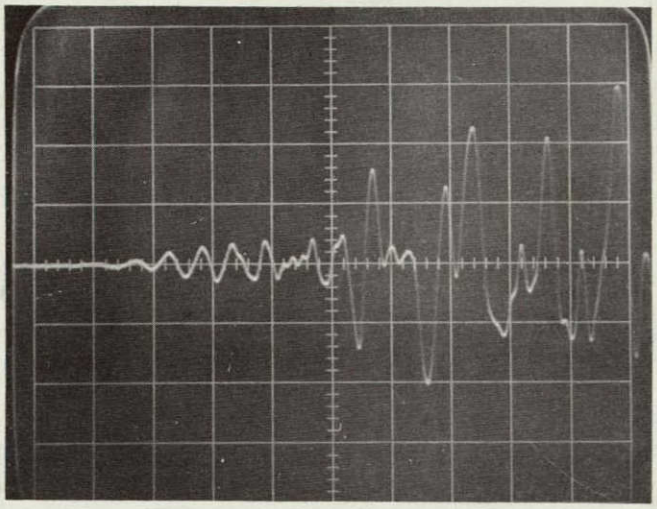

e. 30 INCHES FROM PULSER

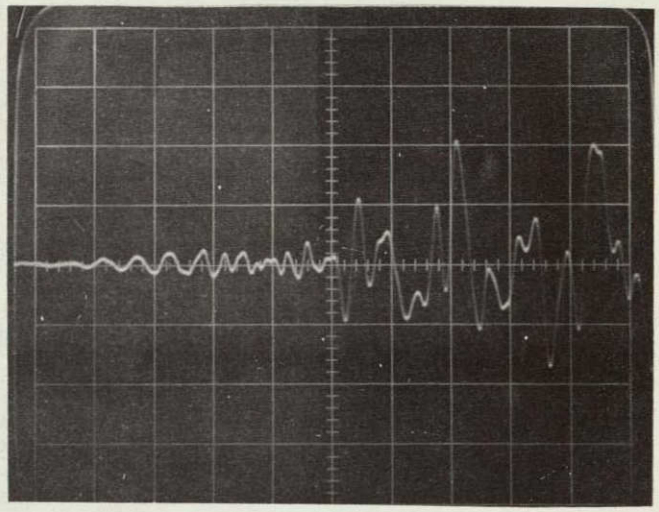

f. 36 INCHES FROM PULSER

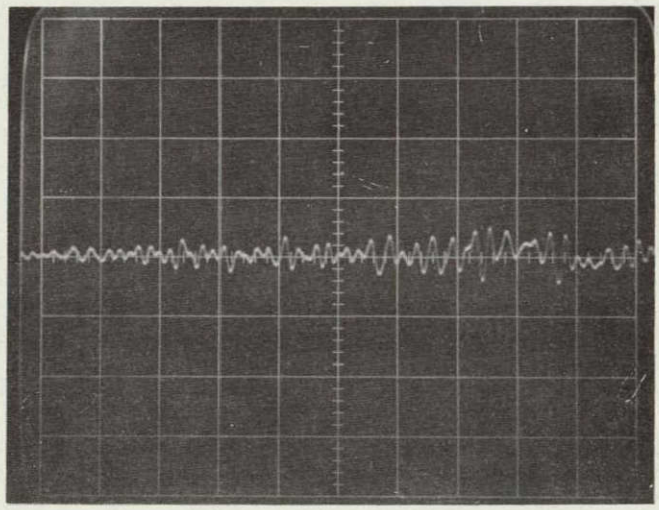

g. 42 INCHES FROM PULSER

T_s = Arrival of Shear Wave

Vertical Scale 1 DIV = 0.1 Volt
Horizontal Scale 1 DIV = 20 μ Sec

Figure 28. Oscillograph Traces for Plate Tests (Sheet 2 of 2)

data. These reflections were received in Tests 5 to 8 because of the relatively small plate that was available for this test series.

TABLE VII

SIGNAL AMPLITUDE VS DISTANCE - PLATE TESTS

Test	Distance from Pulse, in.(x)	Average Amplitude in 20 μ sec, mv
1	6	150
2	12	110
3	18	70
4	24	45

The following statistical analysis was performed to determine the values of C and α in Equation 4.

Test	Distance from Pulse, in. (x)	y, m v	$1_n y$	Y	Y^2	X	X^2	XY	$x.1_n y$
1	6	150	5.00	+0.56	0.314	-9	81	-5.02	30.00
2	12	110	4.70	+0.26	0.067	-3	9	-0.78	56.40
3	18	70	4.25	-0.19	0.036	+3	9	-0.57	76.50
4	24	45	3.81	-0.63	0.397	+9	81	-5.67	91.49
	60		17.76		0.814		180	-12.04	254.39

$$\bar{x} = \frac{60}{4} = 15 \qquad 1_n\bar{y} = \frac{17.76}{4} = 4.44$$

$$\alpha = \frac{\Sigma\, YX}{\Sigma\, Y^2} = -\frac{12.04}{180} = +0.067$$

$$1_n C = 1_n\bar{y} + (0.067)(15) = 4.44 + 0.067(15)$$

$$= 4.44 + 1.00 = 5.44$$

$$C = 230 \text{ mv}$$

V, B, Laboratory Signal Attenuation Evaluations (cont.)

Subsequently the values of signal amplitude (y) were statistically corrected as before and the experimentally determined values of y are compared to the results obtained in Table VIII.

TABLE VIII

COMPARISON OF STATISTICALLY CORRECTED AND TEST-DETERMINED VALUES OF SIGNAL AMPLITUDE - PLATE TESTS

Test	Distance from Pulse, in.	$\frac{1}{n}y$	Corrected Signal Amplitude (y), mv	Experimentally Determined Signal Amplitude (y), mv
1	6	5.04	155	150
2	12	4.64	103	110
3	18	4.17	65	70
4	24	3.83	46	45

The computed value of the pulse amplitude at the source at C equals 230 mv. The regression curve and the experimentally determined points are plotted in Figure 29. It should be observed that the attenuation coefficient for the pipe test was $\alpha = 0.0138$ and for the plate test was 0.067. This is due to the much larger rate of front area that the pulse meets in the plate.

C. SENSOR SPACING

The quiescent background noise measurements performed at the test sites, using a 20 to 50 KHz band-pass filter, are:

Pad A Bottle Field - 0.000099g

VAB Bottle Field - 0.000220g

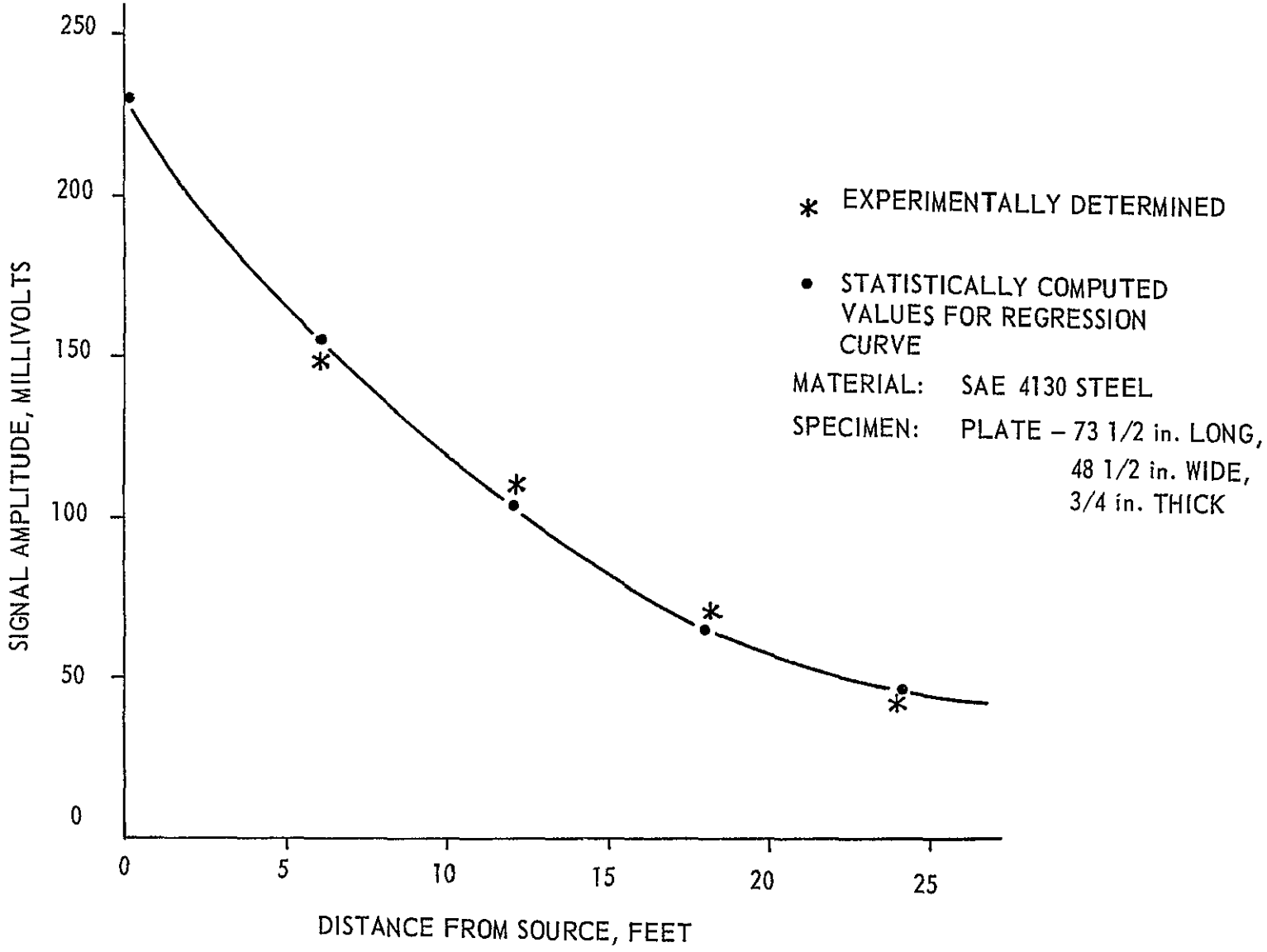

Figure 29. Signal Amplitude vs Distance - Plate Tests

V, C, Sensor Spacing (cont.)

The recorded stress-wave-emission data obtained from the A302B steel bend tests made at the Aerojet-General Corporation laboratory show that the minimum acceleration at the source is 0.0012g, the average 0.0022g, and the maximum 0.0039g. Based on the above data and the attenuation factor X = 0.067 determined from the plate tests, the sensor spacings required to detect crack growth in the vessels at the Kennedy Space Center were computed and the results are tabulated below:

Amplitude at the Source(C), g	Quiescent Background Amplitude(y), g	C/y	l_n(C/y)	Sensor Spacing l_n(C/y), in.
Pad A				
Min Signal 0.0012	0.00015*	8.00	2.08	31.0
Avg Signal 0.0022	0.00015*	14.70	2.69	40.2
Max Signal 0.0039	0.00015*	26.00	3.26	48.7
VAB Bottle Field				
Min Signal 0.0012	0.00033**	3.63	1.29	19.3
Avg Signal 0.0022	0.00033**	6.68	1.90	28.3
Max Signal 0.0039	0.00033**	10.80	2.38	35.6

*This threshold is 1.5 x 0.000099 = 0.00015g (at Pad A).
**This threshold is 1.5 x 0.00022 = 0.00033g (at VAB Bottle Field).

Figures 30 and 31 present schematically the location and spacings of sensors on the pressure vessels.

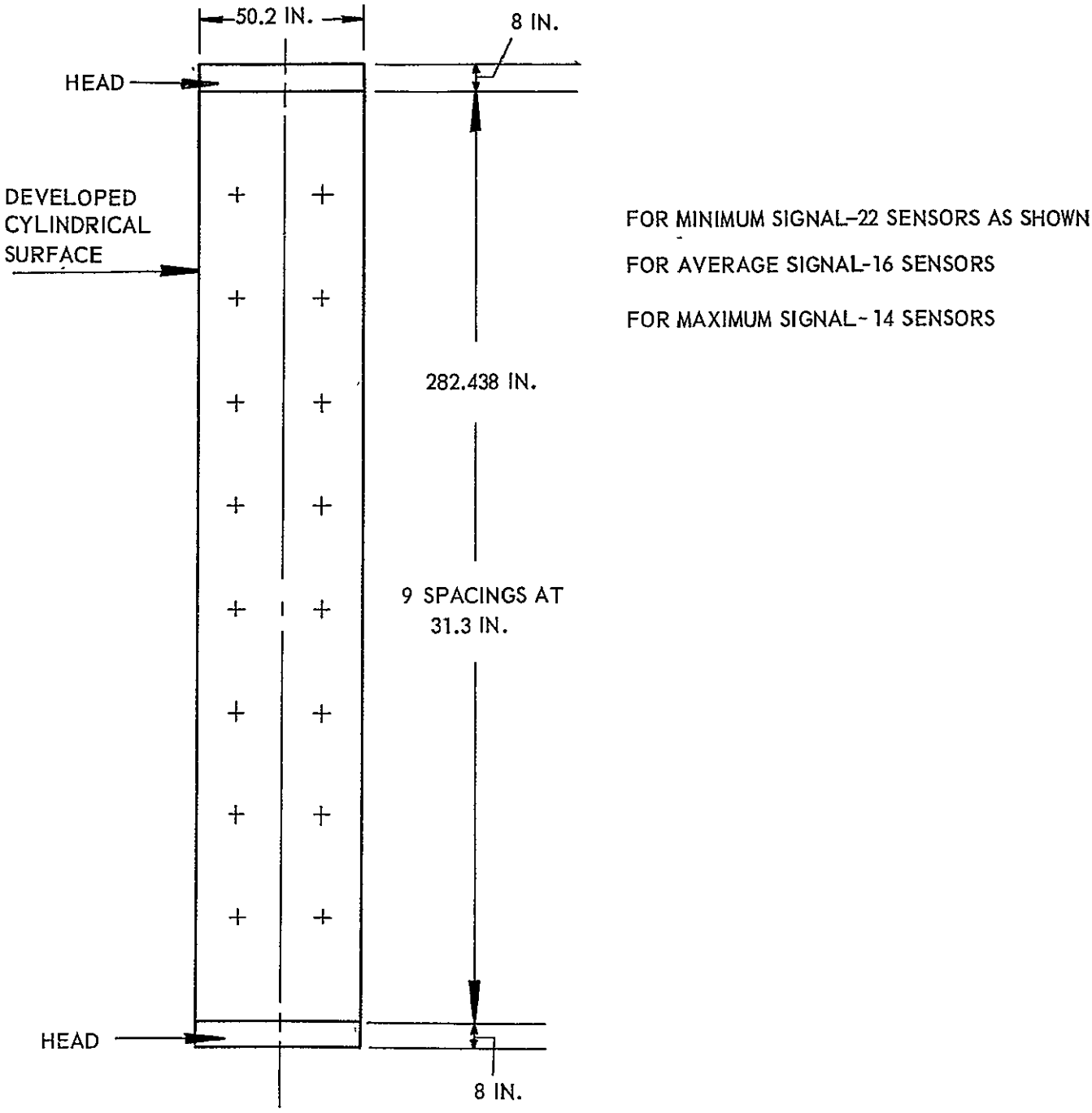

Figure 30. Schematic of Sensor Spacings for Bottles at Pad A

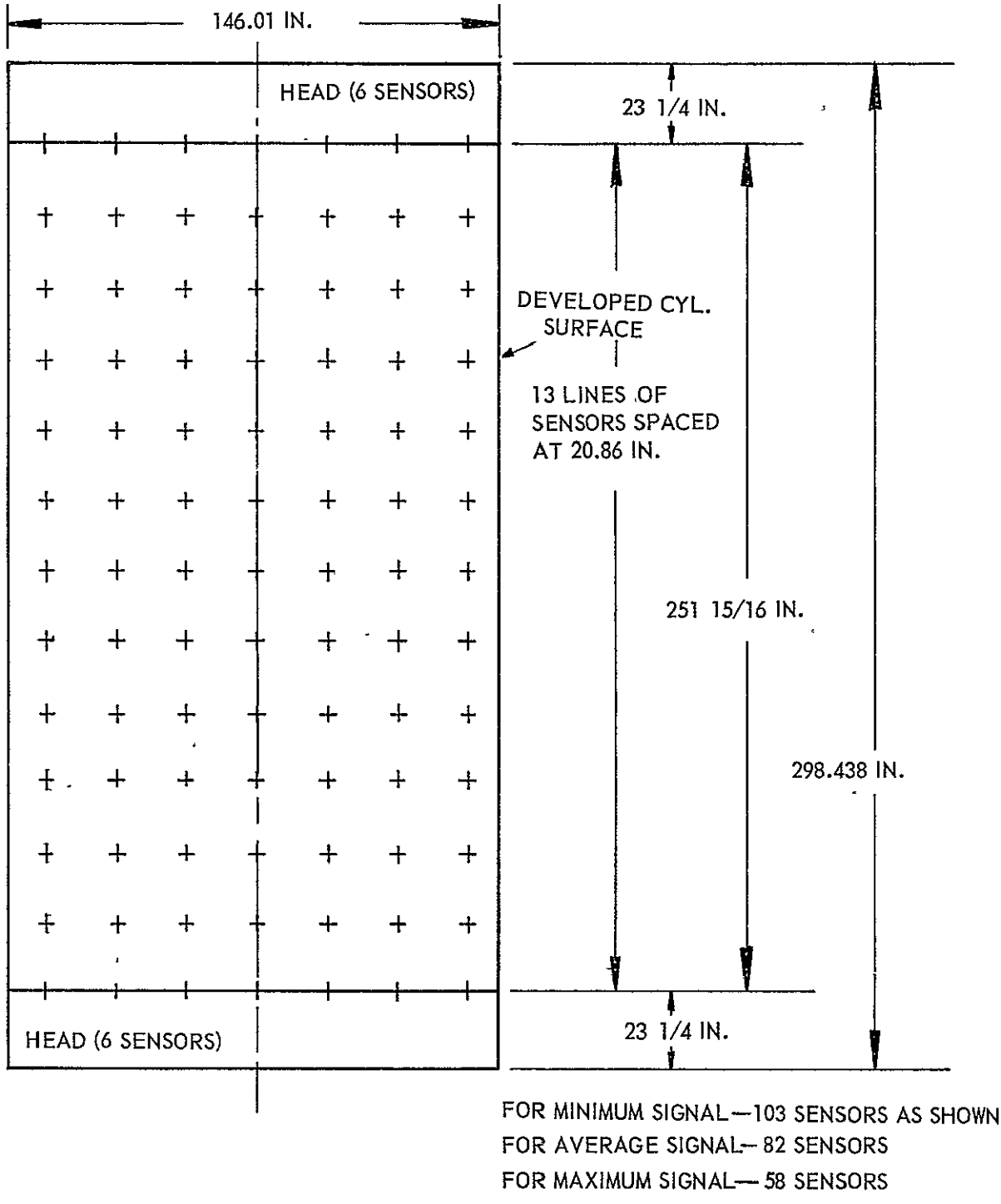

Figure 31. Schematic of Sensor Spacings for Bottles at VAB Bottle Field

VI. CONCLUSIONS

A. The Type A302B steel supplied for evaluation exhibited a high level of fracture toughness. Although "quantitative" plane-strain fracture toughness measurements were not possible because of the large specimen size required, the K_Q value associated with failure approximated 135 ksi-in.$^{1/2}$.

B. The Type A302B steel was found resistant to environmentally induced slow crack growth when tested in the hydrogenated condition in an air environment and in the unhydrogenated condition in a 3% NaCl-water environment. However, hydrogenated material tested in 3% NaCl-water had a much faster rate of subcritical crack growth, indicating a synergistic effect due to the combination of sea water and hydrogen in interstitial solid solution.

C. The synergistic effect indicates the Type A302B steel hydrogen storage tanks in the Kennedy Space Flight Center may have limited life as a result of subcritical crack growth if subjected to the same combination of stress and environmental factors.

D. Detectable stress-wave emissions, although of small amplitude (<0.01g), were observed to be associated with crack growth in Type A302B steel. In all test conditions, the stress-wave emissions were observed during rising load and when failure (instability) was imminent. Both the amplitude and rate of stress-wave emission increased as failure was approached and could be employed as a precursor of the onset of instability.

E. Stress-wave emissions associated with crack growth in Type A302B steel can be detected under quiescent background conditions at the Pad A and VAB Bottle fields at the Kennedy Space Flight Center. However, it would be difficult to detect such stress-wave emissions during tank blowdown and repressurization periods unless filtering can be employed to screen out the noise associated with these periods.

VI, Conclusions (cont.)

F. Even in the presence of background noise from tank blowdown and repressurization, these periods are considered short in the overall life of the pressure vessels. Consequently, flaw growth or "creep", which was observed during rising load or the initial part of hold, could be detected by SWAT, permitting triangulation to the source and tank depressurization prior to failure.

G. Stress-wave-emission attenuation test data were obtained and employed in conjunction with the site background measurements and bend test stress-wave-emission characterization data to determine sensor mounting patterns for the hydrogen pressure vessels at Pad A and the VAB Bottle Field.

VII. RECOMMENDATIONS FOR FURTHER WORK

If the synergistic effect of hydrogen and 3% NaCl solution occurs in Kennedy Space Flight Center tankage, the life of the tankage will be limited. Obviously, slow-crack growth from any cause, whether continuous or discontinuous and regardless of how slow the rate of cracking, will eventually produce failure. This investigation showed that subcritical crack growth is in all likelihood occurring with each pressurization. A question remains, however, as to the rate of crack growth; without knowledge of the rate, there is no way to anticipate the life of the tankage. However, with SWAT one can monitor the occurrence of crack growth and, most importantly, make judgment as to whether a given crack is approaching critical size. Consequently, it is recommended that additional tests be performed to (1) verify the existence of subcritical cracking in actual on-site tankage and (2) incorporate an automatic system for continuously monitoring on-site tankage at Kennedy Space Flight Center.

REFERENCES

1 Steel, R. K., Green, A. T., Lockman, C. S., "Acoustic Verification of Structural Integrity of Polaris Chambers", Society of Plastic Engineers 20th Meeting, Atlantic City, N. Y., January 1964.

2 Pressure Testing of AFRM-017 Service Propulsion System Fuel Tank Utilizing Aerojet-General Corporation's Stress-Wave Analysis Technique, Report NAS 9-6766-003, Aerojet-General Corp. for NASA, MSC, Houston, Texas, Contract NAS 9-6766, May 1967.

3 Srawley, J. E., and Esgar, J. B., Investigation of Hydrotest Failure of Thiokol Chemical Corp. 260-Inch-Diameter SL-1 Motor Case, NASA-TMX - 1194, January 1964.

4 Hartbower, C. E., Gerberich, W. W., and Crimmins, P. P., Mechanisms of Slow Crack Growth in High-Strength Steels, AFML-TR-67-26, Vol 1, February 1967.

5 Hartbower, C. E., Gerberich, W. W., and Crimmins, P. P., Characterization of Fatigue-Crack Growth by Stress Wave Emission, Final Report on Contract NAS 1-4902 for NASA-Langley Research Center, Hampton, Virginia, June 1966.

6 Hartbower, C. E., Gerberich, W. W., Reuter, W. G., and Crimmins, P. P., Stress Wave Characteristics in Constructional Alloys, Final Report on Office of Naval Research Contract N00014-66-C-0340, July 1967.

7 Novak, S. R., and Rolfe, S. T., "Modified WOL Specimen for K_{Iscc} Environmental Testing", U. S. Steel Corp. paper submitted to ASTM for publication.